UNIVERSITY OF CALIFORNIA SAN DIEGO

Understanding the Functional Role of Protein Palmitoylation in Disease

A dissertation submitted in partial satisfaction of the requirements for the degree Doctor of Philosophy

in

Biomedical Sciences

by

Hetika Vora

Committee in charge:

Professor Neal Devaraj, Chair
Professor J. Silvio Gutkind
Assistant Professor Matthew Hangauer
Professor Susan Taylor
Professor Jin Zhang

2021

The dissertation of Hetika Vora is approved, and it is acceptable in quality and form for publication on microfilm and electronically.

University of California San Diego

2021

DEDICATION

I would like to dedicate my doctoral dissertation to my family, who has supported me in all my academic and personal endeavors. Thank you for the love and encouragement you all have given me throughout my life.

EPIGRAPH

We keep moving forward, opening new doors, and doing new things, because we're curious and curiosity keeps leading us down new paths.

Walt Disney

TABLE OF CONTENTS

Dissertation Approval Page……. iii

Dedication…… iv

Epigraph…… v

Table of Contents……. vi

List of Figures…….. ix

List of Schemes…… xi

List of Tables…….. xii

Acknowledgements……... xiii

Vita…….. xv

Abstract of the Dissertation…… xvi

Chapter 1: Introduction……..... 1

1.1 Introduction to Protein S-Palmitoylation…….. 1

1.2 Ras Post-Translational Modifications and Cancer…… 2

1.3 Viral Spike Glycoprotein Palmitoylation and COVID-19…… 4

1.4 References……. 6

Chapter 2: Inhibition of NRAS Signaling in Melanoma Through Direct Depalmitoylation Using Amphiphilic Nucleophiles…….. 9

2.1 Abstract……. 9

2.2 Introduction……..……. 9

2.3 Results……. 12

2.3.1 Depalmitoylation of NRAS in NRAS-Driven Melanoma……... 12

2.3.2 Delocalization of NRAS from the Plasma Membrane……. 16

2.3.3 Inhibition of RAS Signaling in NRAS-Mutated Melanoma…… 18

2.3.4 Reduction of Cell Viability in NRAS-Driven Melanoma…… 22

2.3.5 Apoptosis Induction in NRAS-Driven Melanoma Tumors……. 26

2.3.6 Tumor Growth Decrease in NRAS Melanoma Xenografts……. 28

2.4 Discussion……... 30

2.5 Materials and Methods…… 33

2.5.1 Cell Culture…….. 33

2.5.2 Plasmid Construction and Cloning…….. 33

2.5.3 Generation of Stable Cell Lines……... 35

2.5.4 Live-Cell Imaging of Stable HeLa S3 Cells…… 35

2.5.5 Microscopy…….. 36

2.5.6 S-palmitoylation Acyl-RAC Assay……. 36

2.5.7 Western Blots……... 37

2.5.8 Cell Viability Assay……. 38

2.5.9 Animal Model…….. 39

2.5.10 Histology and Immunohistochemistry……... 39

2.5.11 Alanine Aminotransferase (ALT) Activity…… 40

2.6 Synthesis of Alkyl Reagents……... 40

2.6.1 General Considerations for Synthesis…….. 41

2.6.2 Synthesis of H_2N-*L*-Cys-Oct (1)…….. 44

2.6.3 Synthesis of H_2N-*L*-Ser-Oct (2))…… 44

2.6.4 Synthesis of *N*-Boc-*L*-Cys(Trt)-But)……... 44

2.6.5 Synthesis of H_2N-*L*-Cys-But ∪ H_2N-*L*-Cys-But (3')*…… 44

2.6.6 Synthesis of H_2N-*L*-Cys-But (3)…….. 45

2.6.7 Synthesis of *N*-Boc-*L*-Cys(Trt)-Dodec…… 45

2.6.8 Synthesis of H_2N-*L*-Cys-Dodec ∪ H_2N-*L*-Cys-Dodec (4')*……... 46

2.6.9 Synthesis of H_2N-*L*-Cys-Dodec (4)…… 47

2.6.10 Synthesis of *N*-Boc-*L*-Cys(Trt)-Hexadec…….. 47

2.6.11 Synthesis of H_2N-*L*-Cys-Hexadec ∪ H_2N-*L*-Cys-Hexadec (5')*…….. 48

2.6.12 Synthesis of H_2N-*L*-Cys-Hexadec (5)…… 48

2.6.13 Synthesis of *N*-Ac-*L*-Cys(Trt)-Oct…… 49

2.6.14 Synthesis of *N*-Ac-*L*-Cys-Oct (6')*……... 49

2.6.15 Synthesis of *N*-Ac-*L*-Cys-Oct (6)…….. 50

2.7 Acknowledgements……. 51

2.8 References……... 51

Chapter 3: Determination of SARS-CoV-2 Spike Glycoprotein Palmitoylation and its Contribution to Virus-Cell Fusion…….. 56

3.1 Abstract……... 56

3.2 Introduction……. 57

3.3 Results……. 58

3.3.1 Palmitoylation of SARS-CoV-2 Spike Glycoprotein…….. 58

3.3.2 Localization and Membrane Fusion of SARS-CoV-2 Spike Glycoprotein. 63

3.4 Discussion……... 66

3.5 Acknowledgements……. 67

3.6 References……... 67

LIST OF FIGURES

Figure 2.1 C8 Alkyl Cysteine Causes Depalmitoylation of NRAS in NRAS-Driven Melanoma Cells……. 14

Figure 2.2 Depalmitoylation by C8 Alkyl Cysteine in NRAS-Driven Melanoma Cells…….... 14

Figure 2.3 Depalmitoylation of Proteins in NRAS-Driven Melanoma Cells……. 15

Figure 2.4 C8 Alkyl Cysteine Causes Rapid Delocalization of NRAS from the Plasma Membrane…… 17

Figure 2.5 C8 Alkyl Cysteine Inhibits Oncogenic RAS Signaling in NRAS-Mutated Melanoma Cells in a Dose-Dependent Manner……. 19

Figure 2.6 C8 Alkyl Cysteine Inhibits Oncogenic RAS Signaling in NRAS-Mutated Melanoma Cells Compared to BRAF-Mutated Melanoma Cells…….. 20

Figure 2.7 Western Blot Protein Levels in NRAS-Mutated Melanoma vs. BRAF-Mutated Melanoma……. 21

Figure 2.8 Chemical Structures of Alkyl Cysteine Derivatives and Controls……. 24

Figure 2.9 HPLC/ELSD Spectrum…….. 24

Figure 2.10 Cell Viability of Melanoma Cell Lines Treated with Alkyl Cysteine Derivatives and Controls……. 25

Figure 2.11 C8 Alkyl Cysteine Preferentially Reduces Cell Viability in NRAS-Driven versus BRAF-Driven Melanoma…….. 25

Figure 2.12 C8 Alkyl Cysteine Reduces Proliferation and Induces Apoptosis in NRAS-Driven versus BRAF-Driven Melanoma Tumors……. 27

Figure 2.13 C8 Alkyl Cysteine Causes a Decrease in Tumor Growth in NRAS-Mutated Melanoma Xenograft Mice…….. 29

Figure 2.14 Schematic Representation of NRAS Depalmitoylation and Downstream Inhibition by C8 Alkyl Cysteine……. 32

Figure 3.1 Palmitoylation Status of Spike Glycoprotein After Treatment with 2-BP……. 61

Figure 3.2 Palmitoylation Status of Spike Glycoprotein Palmitoylation Mutants……... 62

Figure 3.3 Localization of Spike Glycoprotein After Treatment with 2-BP……...…… 64

Figure 3.4 Localization and Membrane Fusion of Spike Glycoprotein Cluster Mutants……..... 65

LIST OF SCHEMES

Scheme 2.1 Synthesis of Alkyl Cysteine Derivatives……. 43

LIST OF TABLES

Table 3.1 Palmitoylation Mutants in SARS-CoV-2 Spike Glycoprotein……. 60

ACKNOWLEDGEMENTS

I would like to thank my family and friends for their support and encouragement throughout my graduate journey. To my mom, Manisha, thank you for showing me your love by making sure I never had to worry about food or other household responsibilities, even when I couldn't come home on the weekends. To my dad, Dhairyesh, thank you for all your advice related to project management and always being curious to learn more about my research. To my sister, Riddhi, thank you for always keeping me sane and giving me company when we would go out to have a work-life balance. To the love of my life, Krishna, thank you for being patient while I prepared my doctoral dissertation and for always supporting my career goals.

I would like to acknowledge my thesis advisor, Dr. Neal Devaraj, for his guidance and support during my graduate school experience. I am honored to have had the opportunity to conduct my doctoral research work in the lab of such an exceptional scientist. I am very thankful for all the opportunities you have given me to become an independent scientist and pursue my research interests, unique projects, and career goals.

I would like to acknowledge current and former Devaraj lab members for their valuable insights, thoughtful discussions, and friendly presence in the lab. My graduate school experience has been a lot more enjoyable working in the lab and spending time outside of the lab with amazing colleagues like yourself. I would like to thank Christy Cho for being a kind and understanding colleague and friend. I especially want to thank Dr. Andrew Rudd, who has contributed to my growth and development as an independent scientist in many ways. I cannot express my gratitude enough for all your suggestions, feedback, and advice you have given me during your time in the Devaraj lab as well as beyond. I feel very fortunate to have had you as a mentor and colleague as well as continue to be a role model and friend.

I would like to thank my thesis committee members, Dr. J. Silvio Gutkind, Dr. Jin Zhang, Dr. Matthew Hangauer, and Dr. Susan Taylor, as well as my SPAC advisor Dr. Joan Heller Brown for their insightful suggestions, advice, and development of my thesis project. I would also like to thank the Biomedical Sciences graduate program for their guidance and support throughout my graduate studies. I would like to acknowledge my funding sources, the Molecular Biophysics Training Grant (NIH Grant T32 GM008326) and the NSF RAPID Grant (Award # 2031068).

Chapter 2, in full, is a reprint of the material as it appears in the publication Vora, H. D., Johnson, M., Brea, R. J., Rudd, A. K., and Devaraj N. K. (2020) Inhibition of NRAS Signaling in Melanoma through Direct Depalmitoylation Using Amphiphilic Nucleophiles. *ACS Chem. Biol. 15*, 2079-2086. The dissertation author is the primary investigator and author of this paper.

VITA

Education

2021 Doctor of Philosophy, Biomedical Sciences, University of California San Diego

2016 Bachelor of Science, Pharmaceutical Sciences, University of California Irvine

Publications

Vora, H. D., Johnson, M., Brea, R. J., Rudd, A. K., and Devaraj N. K. (2020) Inhibition of NRAS Signaling in Melanoma through Direct Depalmitoylation Using Amphiphilic Nucleophiles. *ACS Chem. Biol. 15*, 2079-2086.

ABSTRACT OF THE DISSERTATION

Understanding the Functional Role of Protein Palmitoylation in Disease

by

Hetika Vora

Doctor of Philosophy in Biomedical Sciences

University of California San Diego, 2021

Professor Neal Devaraj, Chair

Protein S-palmitoylation is an essential post-translational modification that regulates protein structure and function. It consists of the attachment of a palmitic acid to one or more cysteine residues through a thioester linkage. In cellular proteins, S-palmitoylation plays an important role in membrane localization, trafficking, lipid raft association, and cell signaling. Various viral proteins are also modified with S-palmitoylation; however, their functional role

differs from that of cellular proteins. One of the main differences is that S-palmitoylation is a reversible process in cellular proteins, which allows for recycling and regulation of protein function, whereas in viral proteins, there is no functional benefit to recycle and reuse proteins after viral entry and infection has occurred. The unique nature of S-palmitoylation on protein function makes it an interesting lipid post-translational modification to further characterize and potentially target for therapeutic purposes. There are not many studies that have focused on S-palmitoylation as a targeted therapeutic approach, which makes it even more intriguing to fully understand its effects on cellular and viral proteins. In this dissertation, I examined the effects of directly targeting S-palmitoylation of the NRAS protein, which is highly mutated in multiple cancers including melanoma, using a novel amphiphile-mediated depalmitoylation approach. I discovered that this chemoselective strategy causes delocalization of NRAS from the plasma membrane, inhibition of downstream oncogenic signaling pathways in NRAS-mutated melanoma cells, and reduction of tumor growth in NRAS-mutated melanoma xenograft mice. Additionally, I focused on understanding the role of S-palmitoylation on the SARS-CoV-2 spike glycoprotein. I determined the essential sites of palmitoylation within the C-terminal cysteine-rich region as well as the palmitoylation-dependence of membrane fusion between the spike protein and the host ACE2 receptor. Taken together, these studies highlight the significance of S-palmitoylation on cellular proteins, such as the effect on NRAS function and downstream signaling, and viral proteins, specifically the role on SARS-CoV-2 spike protein-mediated virus-cell membrane fusion, that are involved in various diseases.

Chapter 1: Introduction

1.1 Introduction to Protein S-Palmitoylation

Protein lipidation is an essential post-translational modification (PTM), in which fatty acids are covalently attached to a variety of proteins[1,2]. Linkage of lipid PTMs increases the hydrophobicity of proteins, affecting protein function, regulation, stability, and structure. One of the important lipid modifications found on hundreds of proteins is S-palmitoylation, which is the attachment of the 16-carbon palmitic acid to one or more cysteine residues through a thioester bond[3]. Many of the proteins that are modified with these lipid species are involved in human diseases, such as metabolic diseases, neurological disorders, and cancer[1].

Protein S-palmitoylation is involved in various functional and regulatory roles, such as membrane localization, cellular trafficking, lipid raft association, and downstream cell signaling processes. Additionally, S-palmitoylation is dynamic in nature since the lipid PTM undergoes cycles of palmitoylation and depalmitoylation for many cellular proteins[3]. In these cases, palmitoylation is regulated by palmitoyl acyltransferases (PATs) that promote attachment of palmitate to proteins and palmitoyl thioesterases that readily cleave off the palmitoylation modification[4–6]. Since dysregulation of palmitoylation is associated with many diseases, there is great interest to understand the role of this protein PTM and develop therapeutics to target the unique lipid modification.

The focus of this doctoral dissertation is to understand the functional role of palmitoylation in proteins associated with various diseases and to pave way for novel approaches of targeting the S-palmitoylation lipid modification. Some of the disease-associated proteins of interest include the Ras family of proteins mutated in cancer, of which this dissertation focuses on using an

amphiphile-mediated approach to target NRAS in the context of NRAS-mutated melanoma, and the viral spike glycoprotein in the novel SARS-CoV-2 coronavirus that emerged at the end of 2019.

1.2 Ras Post-Translational Modifications and Cancer

The Ras proteins are G proteins that function as GTPases and regulate cell growth and survival pathways. The four Ras isoforms, which include HRAS, NRAS, KRAS4a, and KRAS4b, are mutated in more than 30% of all human cancers[7]. Ras proteins are post-translationally modified with lipid moieties on their C-terminal hypervariable regions (HVR), which is the region that distinguishes each isoform from one another[8]. Specifically, all the Ras isoforms undergo farnesylation as the first membrane-targeting modification, which occurs in the cytosol. However, only HRAS, NRAS, KRAS4a undergo palmitoylation as the second membrane-binding signal, which occurs in the Golgi. After these isoforms are palmitoylated, they are transported to the plasma membrane through a secretory pathway[2,9,10]. In contrast, KRAS4b does not undergo a secondary signal for membrane-anchoring because its HVR sequence contains a poly-lysine region that allows for passive diffusion and attachment to the plasma membrane[7–9].

For decades, Ras proteins have been extremely challenging to target through traditional small-molecule therapeutic approaches. Two main reasons for this difficulty were because the Ras proteins do not have deep binding pockets on their surfaces and the fact that the Ras proteins have high binding affinity for GTP in the picomolar range, which would make it difficult for a small-molecular inhibitor to compete within the same GTP-binding pocket[7]. For these reasons, currently approved treatments and therapeutic approaches for targeting Ras proteins in a variety of diseases include targeting upstream proteins and downstream effectors. For example, there are drugs that

target the downstream effectors of Ras, such as RAF and MEK inhibitors. However, there are significant challenges in implementing these treatments long-term, such as leading to resistance and feedback loop activation of upstream signaling through receptor tyrosine kinases (RTKs), which can lead to an increase in other downstream pathways such as the PI3K/AKT signaling pathway[7,9,11]. Although the recent development of mutant-specific inhibitors for KRAS(G12C) have entered phase 2 clinical trials with promising results, the issue of acquired resistance is being studied and more treatment approaches are still needed to target the other Ras isoforms[12–15].

An alternative therapeutic approach to targeting Ras proteins that has gained much interest in the last decade is to target the post-translational modifications of these "undruggable" proteins. Specifically, farnesyl transferase inhibitors (FTIs) have been developed to directly block the enzyme that covalently attaches a farnesyl group to these proteins[16,17]. Recent clinical trials have demonstrated encouraging results showing the FTI tipifarnib is efficacious in patients with head and neck squamous cell carcinoma (HNSCC) with HRAS mutations[18,19]. Although these results show the benefit of taking an alternative, indirect approach to targeting HRAS, FTIs are ineffective in NRAS and KRAS mutant cancers because these two Ras isoforms are alternatively geranylgeranylated when farnesylation is blocked[7,9]. For this reason, there is still great need for effective Ras-targeting therapies, one of which could be to target the palmitoylation modification since there are currently no selective palmitoylation inhibitors.

About one third of all human cancers have activating mutations in RAS oncogenes. In particular, NRAS mutations are found in about 20% of melanomas. NRAS-mutant melanomas are more aggressive, with a higher fatality rate in patients with this subset of skin cancer[20]. Currently, melanoma patients receive immune-based therapies as first-line treatment and chemotherapy as second-line treatment, which are not always effective[21]. It was observed in a small NRAS-mutated

cohort of melanoma patients that there was a response to high-dose interleukin-2; however, about 53% of patients did not have a response to this approved but toxic immunotherapy[22]. Although there is some promising preclinical and clinical data, there is currently no approved treatment that combats NRAS-mutant melanomas with significant survival rates. There is a great need for a targeted therapy for patients with NRAS-mutated melanoma using unique approaches, rather than those currently implemented in the clinic. A possible approach would be to target post-translational modifications of NRAS, such as S-palmitoylation, to prevent the excessive cancer cell growth and survival seen in melanoma. Chapter 2 of this dissertation focuses on using a novel chemoselective approach that our group has developed to target the palmitoylation modification on NRAS and inhibit its downstream signaling in the context of NRAS-mutated melanoma.

1.3 Viral Spike Glycoprotein Palmitoylation and COVID-19

Lipid PTMs, including S-palmitoylation, are not only found in a wide variety of cellular proteins but also in multiple viral proteins[1]. Since viruses rely on the host cell's machinery for replication and protein synthesis, many viral proteins undergo attachment of PTMs[23]. However, the functional roles of S-palmitoylation in viral proteins differs in some ways from its roles in cellular proteins, especially pertaining to its dynamic nature. The typical cycles of palmitoylation and depalmitoylation that occur in cellular proteins has not been observed in viral proteins[24]. This difference may be due to the fact that S-palmitoylation linkage on cellular proteins regulates their localization and function, and thus allows for these proteins to be reused and recycled multiple times. However, in contrast, viral proteins do not need to be reused because they perform their function of viral entry and infection only once[25].

Coronaviruses are a group of enveloped RNA viruses that cause diseases in both humans and animals[23]. This group of viruses are made up of three main transmembrane structural proteins – spike glycoprotein (S), envelope protein (E), and membrane protein (M)[26,27]. The entry and replication cycle of coronaviruses is initiated by the binding of the spike glycoprotein to its host cell surface receptor[23]. This binding event triggers a conformational change in the spike protein that results in the membrane fusion between the virus and host cell.

Many viral proteins, including structural, nonstructural, and accessory proteins, in coronaviruses are modified post-translationally with lipid species, such as fatty acids. The roles and functions of these PTMs affect coronavirus biology as well as virus-host cell interactions[23]. The spike glycoprotein is known to be palmitoylated within the C-terminal cysteine-rich cytosolic tail, which is conserved across multiple coronaviruses[26]. Not many studies have been done to fully characterize S-palmitoylation on coronavirus spike proteins and its effects on viral infection. Depending on the coronavirus, the function and role of palmitoylation may differ when it comes to protein folding, membrane fusion, and protein-protein interactions[23].

The most recent coronavirus that appeared in 2019 is the severe acute respiratory syndrome coronavirus 2 (SARS-CoV-2) that causes COVID-19, a fatal respiratory disease that has caused over 3 million deaths worldwide[28]. With the emergence of this global pandemic, there has been tremendous need for rapid development of vaccines to prevent SARS-CoV-2 viral infection as well as therapeutics for treating individuals who have already been infected with the virus. A unique therapeutic approach could be to focus on the S-palmitoylation modification found on coronavirus spike glycoproteins and determine if removal of this PTM has significant effects on SARS-CoV-2 viral entry. Chapter 3 of this dissertation focuses on understanding the functional role of S-palmitoylation of the novel SARS-CoV-2 spike glycoprotein on virus-cell membrane

fusion that contributes to viral infection. Gaining further insight on the effects of spike protein palmitoylation on viral entry and infection could potentially provide a novel target on this viral protein for the treatment of COVID-19.

1.4 References

(1) Chen, B., Sun, Y., Niu, J., Jarugumilli, G. K., and Wu, X. (2018) Protein Lipidation in Cell Signaling and Diseases: Function, Regulation, and Therapeutic Opportunities. *Cell Chem. Biol. 25*, 817–831.

(2) Resh, M. D. (2012) Targeting protein lipidation in disease. *Trends Mol. Med. 18*, 206–214.

(3) Resh, M. D. (2006) Palmitoylation of Ligands, Receptors, and Intracellular Signaling Molecules. *Sci. STKE 2006*, 14–14.

(4) Linder, M. E., and Deschenes, R. J. (2007) Palmitoylation: Policing protein stability and traffic. *Nat. Rev. Mol. Cell Biol. 8*, 74–84.

(5) Yeste-Velasco, M., Linder, M. E., and Lu, Y. J. (2015) Protein S-palmitoylation and cancer. *Biochim. Biophys. Acta - Rev. Cancer 1856*, 107–120.

(6) Mitchell, D. A., Vasudevan, A., Linder, M. E., and Deschenes, R. J. (2006) Protein palmitoylation by a family of DHHC protein S-acyltransferases. *J. Lipid Res. 47*, 1118–1127.

(7) Simanshu, D. K., Nissley, D. V., and McCormick, F. (2017) RAS Proteins and Their Regulators in Human Disease. *Cell 170*, 17–33.

(8) Ahearn, I. M., Haigis, K., Bar-Sagi, D., and Philips, M. R. (2012) Regulating the regulator: Post-translational modification of RAS. *Nat. Rev. Mol. Cell Biol. 13*, 39–51.

(9) Rajalingam, K., Schreck, R., Rapp, U. R., and Albert, S. (2007) Ras oncogenes and their downstream targets. *Biochim. Biophys. Acta - Mol. Cell Res. 1773*, 1177–1195.

(10) Xiang, S., Bai, W., Bepler, G., and Zhang, X. (2017) Activation of Ras by Post-Translational Modifications. *Conqu. RAS*. Elsevier Inc.

(11) Papke, B., and Der, C. J. (2017) Drugging RAS: Know the enemy. *Science (80-.). 355*, 1158–1163.

(12) Ostrem, J. M., Peters, U., Sos, M. L., Wells, J. A., and Shokat, K. M. (2013) K-Ras(G12C) inhibitors allosterically control GTP affinity and effector interactions. *Nature 503*, 548–551.

(13) Canon, J., Rex, K., Saiki, A. Y., Mohr, C., Cooke, K., Bagal, D., Gaida, K., Holt, T., Knutson, C. G., Koppada, N., Lanman, B. A., Werner, J., Rapaport, A. S., San Miguel, T., Ortiz, R., Osgood, T., Sun, J. R., Zhu, X., McCarter, J. D., Volak, L. P., Houk, B. E., Fakih, M. G., O'Neil, B. H., Price, T. J., Falchook, G. S., Desai, J., Kuo, J., Govindan, R., Hong, D. S., Ouyang, W., Henary, H., Arvedson, T., Cee, V. J., and Lipford, J. R. (2019) The clinical KRAS(G12C) inhibitor AMG 510 drives anti-tumour immunity. *Nature 575*, 217–223.

(14) McCormick, F. (2020) Sticking it to KRAS: Covalent Inhibitors Enter the Clinic. *Cancer Cell 37*, 3–4.

(15) Nagasaka, M., Li, Y., Sukari, A., Ou, S.-H. I., Al-Hallak, M. N., and Azmi, A. S. (2020) KRAS G12C Game of Thrones, which direct KRAS inhibitor will claim the iron throne? *Cancer Treat. Rev. 84*, 101974.

(16) Berndt, N., Hamilton, A. D., and Sebti, S. M. (2011) Targeting protein prenylation for cancer therapy. *Nat. Rev. Cancer 11*, 775–791.

(17) Gajewski, T. F., Salama, A. K. S., Niedzwiecki, D., Johnson, J., Linette, G., Bucher, C., Blaskovich, M. A., Sebti, S. M., and Haluska, F. (2012) Phase II study of the farnesyltransferase inhibitor R115777 in advanced melanoma (CALGB 500104). *J. Transl. Med. 10*, 1–8.

(18) Gilardi, M., Wang, Z., Proietto, M., Chilla, A., Calleja-Valera, J. L., Goto, Y., Vanoni, M., Janes, M. R., Mikulski, Z., Gualberto, A., Molinolo, A. A., Ferrara, N., Silvio Gutkind, J., and Burrows, F. (2020) Tipifarnib as a precision therapy for HRAS-mutant head and neck squamous cell carcinomas. *Mol. Cancer Ther. 19*, 1784–1796.

(19) Ho, A. L., Brana, I., Haddad, R., Bauman, J., Bible, K., Oosting, S., Wong, D. J., Ahn, M.-J., Boni, V., Even, C., Fayette, J., Flor, M. J., Harrington, K., Kim, S.-B., Licitra, L., Nixon, I., Saba, N. F., Hackenberg, S., Specenier, P., Worden, F., Balsara, B., Leoni, M., Martell, B., Scholz, C., and Gualberto, A. (2021) Tipifarnib in Head and Neck Squamous Cell Carcinoma With HRAS Mutations . *J. Clin. Oncol. 39*, 1856–1864.

(20) Muñoz-Couselo, E., Adelantado, E. Z., Ortiz, C., García, J. S., and Perez-Garcia, J. (2017) NRAS-mutant melanoma: Current challenges and future prospect. *Onco. Targets. Ther. 10*, 3941–3947.

(21) Boespflug, A., Caramel, J., Dalle, S., and Thomas, L. (2017) Treatment of NRAS - mutated advanced or metastatic melanoma: Rationale, current trials and evidence to date. *Ther. Adv. Med. Oncol. 9*, 481–492.

(22) Johnson, D. B., and Puzanov, I. (2015) Treatment of NRAS-Mutant Melanoma. *Curr. Treat. Options Oncol. 16*.

(23) Fung, T. S., and Liu, D. X. (2018) Post-translational modifications of coronavirus proteins: Roles and function. *Future Virol. 13*, 405–430.

(24) Bijlmakers, M. J., and Marsh, M. (2003) The on-off story of protein palmitoylation. *Trends Cell Biol. 13*, 32–42.

(25) Veit, M. (2012) Palmitoylation of virus proteins. *Biol. Cell 104*, 493–515.

(26) Petit, C. M., Chouljenko, V. N., Iyer, A., Colgrove, R., Farzan, M., Knipe, D. M., and Kousoulas, K. G. (2007) Palmitoylation of the cysteine-rich endodomain of the SARS-coronavirus spike glycoprotein is important for spike-mediated cell fusion. *Virology 360*, 264–274.

(27) McBride, C. E., and Machamer, C. E. (2010) Palmitoylation of SARS-CoV S protein is necessary for partitioning into detergent-resistant membranes and cell-cell fusion but not interaction with M protein. *Virology 405*, 139–148.

(28) Dong, E., Du, H., and Gardner, L. (2020) An interactive web-based dashboard to track COVID-19 in real time. *Lancet Infect. Dis. 3099*, 19–20.

Chapter 2: Inhibition of NRAS Signaling in Melanoma Through Direct Depalmitoylation Using Amphiphilic Nucleophiles

2.1 Abstract

Activating mutations in the small GTPase NRAS are responsible for driving tumor growth in several cancers. Unfortunately, the development of NRAS inhibitors has proven difficult due to the lack of hydrophobic binding pockets on the protein's surface. To overcome this limitation, we chose to target the posttranslational S-palmitoyl modification of NRAS, which is required for its signaling activity. Utilizing an amphiphile-mediated depalmitoylation (AMD) strategy, we demonstrate the ability to directly cleave S-palmitoyl groups from NRAS and inhibit its function. C8 alkyl cysteine causes a dose-dependent decrease in NRAS palmitoylation and inhibits downstream signaling in melanoma cells with an activating mutation in NRAS. This compound reduces cell growth in NRAS-driven versus non-NRAS-driven melanoma lines and inhibits tumor progression in an NRAS-mutated melanoma xenograft mouse model. Our work demonstrates that AMD can effectively suppress NRAS activity and could represent a promising new avenue for discovering lead compounds for treatment of NRAS-driven cancers.

2.2 Introduction

Ras proteins are small GTPases that regulate many cellular events including proliferation[1], differentiation[2], adhesion[3], apoptosis[4], and migration[5]. There are four known isoforms of the Ras family of proteins – NRAS, HRAS, KRAS4a, and KRAS4b – that are mutated in numerous diseases ranging from neurodevelopmental disorders to various cancers[6]. Activating mutations in

the *RAS* oncogenes are found in approximately one third of all cancers[6], making it the most frequently mutated gene family in human cancer.

Ras proteins are very difficult to target and have even been deemed "undruggable"[7]. Small-molecule inhibitors that directly bind to Ras proteins with high affinity are extremely challenging to develop due to the lack of deep binding pockets on their surfaces[6], though recent breakthroughs have been made for the G12C mutant through use of covalent inhibitors[8,9]. Because of this complexity, current treatments and therapeutic approaches for targeting Ras-related diseases rely on targeting upstream proteins and downstream effectors. However, these approaches often come with significant challenges such as feedback loop activation or acquired resistance[10].

Membrane anchoring post-translational modifications (PTMs) on Ras occur at the C-terminal hypervariable region (HVR)[11]. These PTMs are involved in regulation of cell signaling pathways as well as membrane localization, cellular trafficking, and activation of Ras proteins[6,12,13]. Membrane localization of Ras proteins is necessary for their downstream signaling events to occur[6]. The membrane localization of NRAS, HRAS, and KRAS4a is regulated by prenylation and palmitoylation at the CAAX terminus, which creates a hydrophobic lipid domain on the C-terminal cysteine[6]. On the other hand, KRAS4b is not palmitoylated but rather contains a polybasic region in its HVR allowing for its passive diffusion to the plasma membrane[6,12,13]. NRAS and HRAS are palmitoylated by the palmitoyl acyltransferase (PAT) enzyme DHHC9-GPC16 complex and depalmitoylated by acyl-protein thioesterases, which allow for their release from the plasma membrane and diffusion back to the Golgi[14,15].

A potential therapeutic strategy to target oncogenic Ras isoforms in cancers would be to prevent membrane association by direct targeting of lipid PTMs, such as prenylation or palmitoylation. The first small-molecule inhibitors developed to target PTMs of Ras proteins were

farnesyltransferase inhibitors (FTIs), which directly blocked the farnesyl transferase enzyme by competitively binding to the CAAX binding site[16]. These FTIs inhibited HRAS farnesylation and membrane localization in cells, which decreased cell growth in various human cancer cell lines[6]. However, although FTIs seem to have promising effects on certain HRAS mutant cancers in recent clinical trials, they failed to work for all of the Ras isoforms[17,18]. This result was explained by the fact that NRAS, KRAS4a, and KRAS4b were found to undergo geranylgeranylation as an alternative prenylation modification when farnesylation was blocked by FTIs[6,12].

Due to the ineffectiveness of FTIs for NRAS, a good alternative approach would be to target palmitoylation, since there are no known compensatory mechanisms for lipidating S-palmitoylation sites if PATs are blocked. Currently, there are no selective inhibitors for palmitoylation because of the difficulty to target only one of the 23 PAT enzymes and their overlapping substrate specificity[15,16,19]. However, the irreversible inhibitor 2-bromopalmitate (2-BP) has been used as a pharmacological tool to study protein palmitoylation for many years[11,19]. Because 2-BP is a promiscuous electrophile, it targets multiple enzymes involved in lipid metabolism as well as many other proteins and non-CoA-dependent enzymes, which limits its potential as a therapeutic candidate for depalmitoylation due to off-target side effects and associated toxicity issues[20]. Thus, it would be beneficial to take an alternative approach to traditional enzymatic inhibitors and use a chemoselective chemical agent to directly target palmitoylation of NRAS as a means to suppress its signaling capabilities that are responsible for tumor progression. Recently, our group has developed an amphiphile-mediated depalmitoylation (AMD) strategy using a compound, termed C8 alkyl cysteine (**1**), to cleave S-palmitoyl groups from endogenous membrane-associated proteins[21]. We sought to apply the AMD approach to depalmitoylate NRAS and inhibit its function in the context of an NRAS-driven cancer.

Here we demonstrate that C8 alkyl cysteine (**1**) is able to depalmitoylate NRAS in NRAS-mutated melanoma, leading to significant phenotypic effects *in vitro* and *in vivo*. In turn, depalmitoylation of NRAS decreased phosphorylation of downstream proteins such as AKT and ERK in NRAS-mutated melanoma cells. Fluorescence microscopy studies showed that treatment with the depalmitoylating agent caused delocalization of NRAS from the plasma membrane. We also determined that as concentrations of **1** increased, the cell viability of NRAS-mutated melanoma cell lines decreased, while the cell viability of a BRAF-mutated melanoma cell line was unaffected until much higher concentrations. Cell death was partially rescued by addition of an NRAS mutant bearing a non-palmitoylated membrane binding tail derived from KRAS4b, which is not dependent on palmitoylation for plasma membrane localization. In an NRAS-mutated melanoma xenograft mouse model, treatment with **1** caused a decrease in p-ERK, increase in apoptosis, and decrease in tumor growth. These results suggest that directly depalmitoylating NRAS with **1** can inhibit its downstream signaling pathways involved in NRAS-driven cancers.

2.3 Results

2.3.1 Depalmitoylation of NRAS in NRAS-Driven Melanoma

Based on our group's initial findings that C8 alkyl cysteine (**1**) is able to depalmitoylate membrane-associated proteins in cells[21], we sought to determine if this compound would have similar effects on the palmitoylation state of mutant NRAS. For these initial tests, we used the WM3000 human melanoma cell line, which has an activating Q61R mutation in NRAS[22,23]. We found that 2 hour incubation with increasing concentrations of **1** (Figure 2.1a) resulted in a dose-dependent decrease in the levels of NRAS(Q61R) palmitoylation in cells, with an IC_{50} of 7 μM, as determined by acyl-resin assisted capture (acyl-RAC)[24,25] (Figure 2.1b,c and Figure 2.2a).

Controls were performed in which WM3000 cells were treated with vehicle or C8 alkyl serine (**2**), a structurally similar molecule which is not capable of S-palmitoyl thioester cleavage because it lacks a nucleophilic thiol (Figure 2.1a)[21]. As expected, there was no observable thioester cleavage under these conditions, indicating that the observed reduction in NRAS palmitoylation is due to direct cleavage of the NRAS S-palmitoyl group by **1** and not a non-specific effect of **1** (Figure 2.1d,e). As a positive control, cells treated with the non-specific, irreversible palmitoylation inhibitor 2-BP[11,19,20] also caused a decrease in NRAS palmitoylation (Figure 2.1d,e). However, total protein palmitoylation is significantly decreased when treated with 2-BP compared to **1** as observed by silver staining (Figure 2.2b), which suggests that there is less off-target depalmitoylation with **1.** Additionally, a small panel of known S-palmitoylated proteins were studied after treatment with **1**, **2**, or 2-BP to determine if there were significant decreases in protein palmitoylation levels.[21] Compound **1** showed a preference for NRAS over other tested palmitoylated proteins in this panel. On the other hand, compound **2** did not have observable effects on the palmitoylation of the various proteins, while 2-BP non-selectively caused an overall decrease in protein palmitoylation (Figure 2.3a,b). With this information, we confirmed biochemically that compound **1** is able to depalmitoylate NRAS in NRAS-mutated melanoma cells through direct nucleophilic cleavage of the S-palmitoyl thioester.

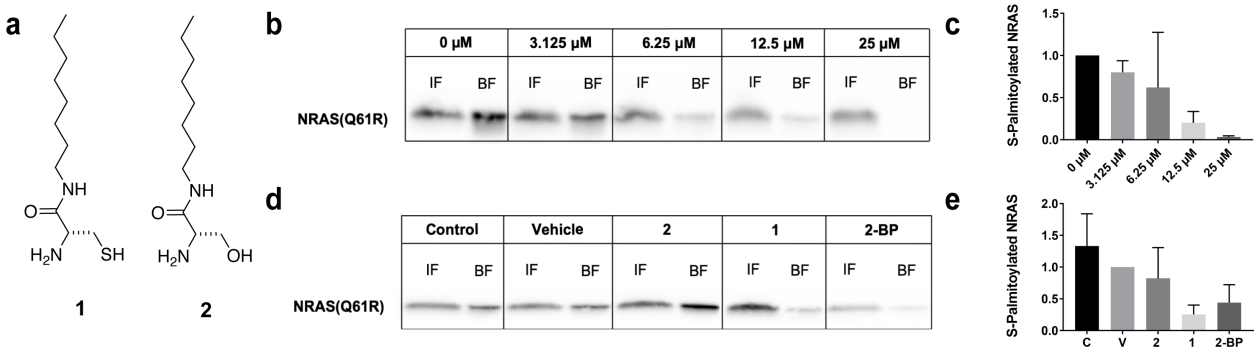

Figure 2.1 C8 Alkyl Cysteine Causes Depalmitoylation of NRAS in NRAS-Driven Melanoma Cells. **(a)** Chemical structures of C8 alkyl cysteine (**1**) and control compound C8 alkyl serine (**2**). **(b)** Western blot detection of NRAS Q61R in acyl resin-assisted capture fractions of WM3000 melanoma cells after treatment with increasing concentrations (0–25 μM) of C8 alkyl cysteine (**1**). Input fractions (IF) contain total cellular protein and bound fractions (BF) contain only S-palmitoylated proteins. **(c)** Western blot lanes were analyzed and quantified using ImageJ. Ratios of BF to IF for each of the treatment conditions were calculated and normalized to the 0 μM control to determine the amount of S-palmitoylated NRAS in each sample. Results are the mean ± s.d. of three independent experiments (one-way ANOVA). **(d)** WM3000 melanoma cells were treated with different conditions, including the untreated control (C), vehicle control (20 μM TCEP in DMSO) (V), 10 μM C8 alkyl serine (**2**), 10 μM C8 alkyl cysteine (**1**), and 10 μM 2-bromopalmitate (2-BP) for 2 hours. **(e)** Ratios of BF to IF for each of the treatment conditions were calculated and normalized to vehicle control to determine the amount of S-palmitoylated NRAS in each sample. Results are the mean ± s.d. of three independent experiments (one-way ANOVA).

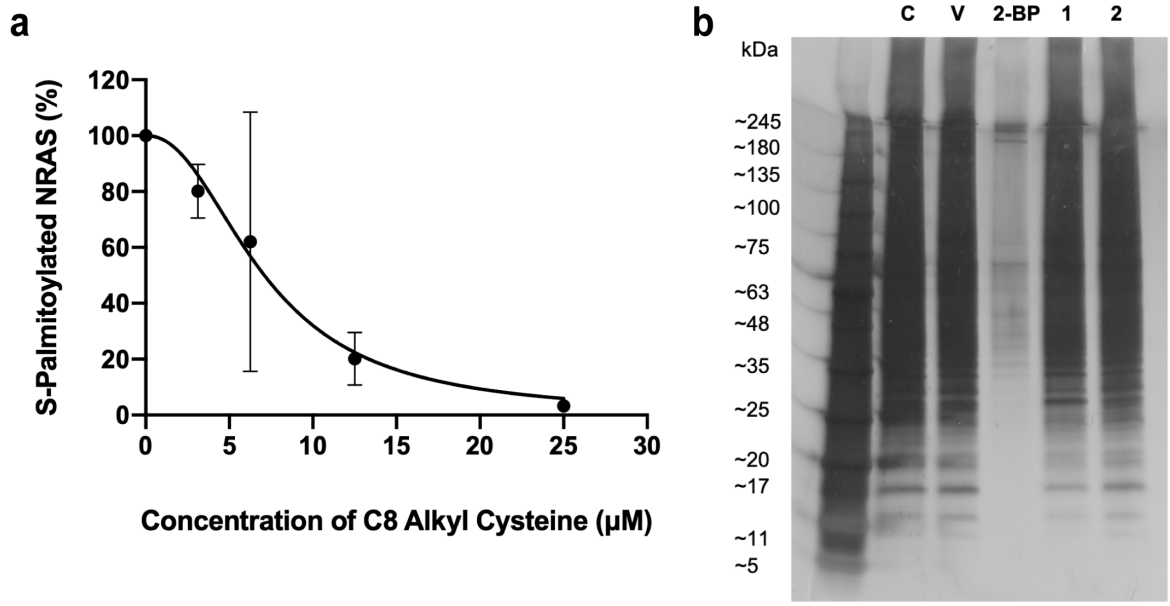

Figure 2.2 Depalmitoylation by C8 Alkyl Cysteine in NRAS-Driven Melanoma Cells. **(a)** Western blot analysis of WM3000 NRAS-mutated melanoma cells after treatment with increasing concentrations (0–25 μM) of C8 alkyl cysteine (**1**) from Figure 1c. Nonlinear regression (curve fit) with variable slopes was used to determine IC_{50}. Results are the mean ± SEM of three independent experiments. **(b)** Silver staining of S-palmitoylated proteins in WM3000 NRAS-mutated melanoma. Treatment conditions include the untreated control (C), vehicle control (20 μM TCEP in DMSO) (V), 10 μM 2-bromopalmitate (2-BP), 10 μM C8 alkyl cysteine (**1**), and 10 μM C8 alkyl serine (**2**). All samples were from the acyl resin-assisted capture (acyl-RAC) bound fractions (BF) that contain only S-palmitoylated proteins from Figure 1d.

Figure 2.3 Depalmitoylation of Proteins in NRAS-Driven Melanoma Cells. **(a)** Western blot detection of palmitoylated proteins in acyl resin-assisted capture fractions of WM3000 melanoma cells after 2-hour treatment with vehicle (20 μM TCEP in DMSO), 10 μM C8 alkyl cysteine (**1**), 10 μM C8 alkyl serine (**2**), or 10 μM 2-bromopalmitate (2-BP). Input fractions (IF) contain total cellular protein and bound fractions (BF) contain only S-palmitoylated proteins. **(b)** Western blot lanes were analyzed and quantified using ImageJ. Ratios of BF to IF for each treatment condition were calculated and normalized to vehicle to determine the amount of the S-palmitoylated proteins in each sample.

2.3.2 Delocalization of NRAS from the Plasma Membrane

To understand the biological effects of compound **1** on NRAS after depalmitoylation, we investigated the change in subcellular localization that occurred after treatment using fluorescence microscopy. Previous studies have shown that S-palmitoylation is required for NRAS anchorage to the plasma membrane[26,27]. Due to their ease of transfection and clear localization of RAS to the plasma membrane, we chose to use HeLa S3 cells as a model to visualize changes in NRAS localization. HeLa S3 cells stably expressing enhanced green fluorescent protein (EGFP)-tagged NRAS were treated with 20 μM of **1**. We observed the delocalization of EGFP-NRAS from the plasma membrane within 30 minutes of treatment with **1** (Figure 2.4a,b), whereas there was no change in localization after treatment with the control **2** (Figure 2.4c,d). We also treated cells with 20 μM of 2-BP, which was expected to non-specifically inhibit palmitoylation. Although the results showed a partial delocalization of the EGFP-NRAS from the plasma membrane, there was no observation of an increase in localization at the Golgi[28] (Figure 2.4e,f). This result may be attributed to the fact that 2-BP irreversibly inhibits palmitoylation and targets multiple other metabolic enzymes[20]. Additionally, 2-BP would not remove already palmitoylated NRAS from the plasma membrane, but rather it would only inhibit NRAS from being palmitoylated at the Golgi. This highlights the difference between direct depalmitoylation using **1** and inhibition of palmitoylation using 2-BP. The localization experiments confirmed that **1** causes NRAS to delocalize from the plasma membrane after depalmitoylation.

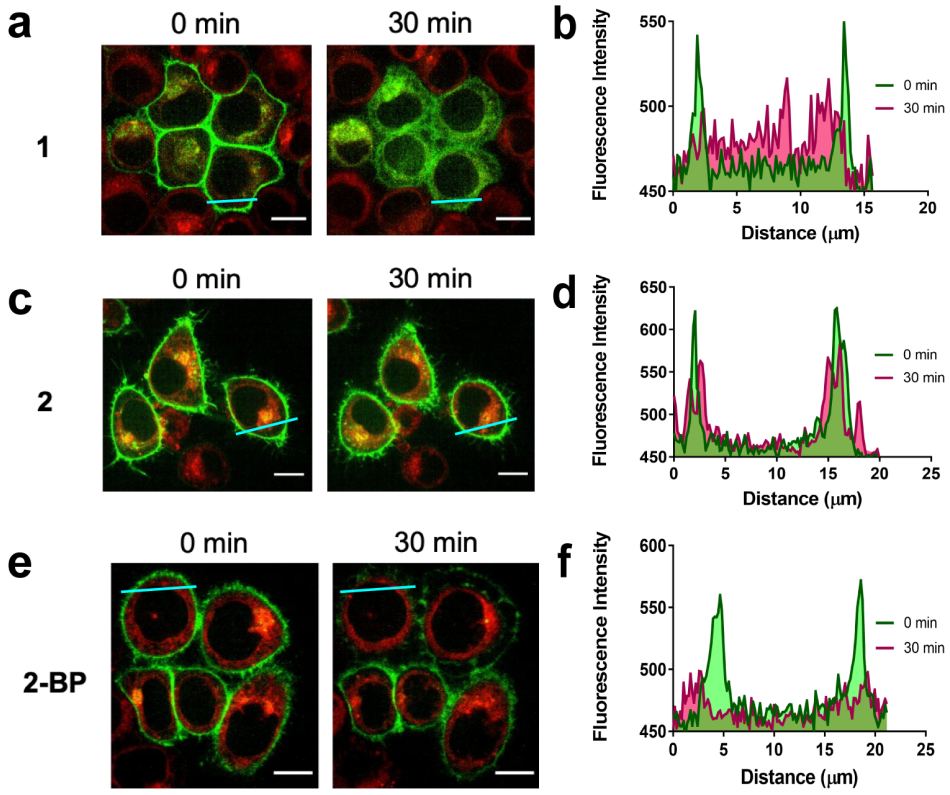

Figure 2.4 C8 Alkyl Cysteine Causes Rapid Delocalization of NRAS from the Plasma Membrane. **(a)** EGFP-NRAS plasmid was stably transfected in HeLa S3 cells and treated with 20 μM C8 alkyl cysteine (**1**) for 30 min to visualize delocalization of NRAS from the plasma membrane. **(b)** Profile plots of cross sections (blue line) show EGFP-NRAS delocalization before (0 min) and after (30 min) treatment with **1**. **(c)** EGFP-NRAS HeLa S3 cells were treated with 20 μM of the control C8 alkyl serine (**2**) for 30 min. **(d)** Profile plots of cross sections show EGFP-NRAS delocalization before (0 min) and after (30 min) treatment with **2**. **(e)** EGFP-NRAS HeLa S3 cells were treated with 20 μM 2-bromopalmitate (2-BP) for 30 min. **(f)** Profile plots of cross sections show EGFP-NRAS delocalization before (0 min) and after (30 min) treatment with 2-BP. NRAS was fused to EGFP (green) and the Golgi apparatus was stained with BODIPY TR Ceramide (red). Scale bars denote 10 μm.

2.3.3 Inhibition of RAS Signaling in NRAS-Mutated Melanoma

Since there was an observable decrease in NRAS palmitoylation and a delocalization of NRAS from the plasma membrane after treatment with **1**, we wanted to study the changes that occur in downstream RAS signaling. It is well known that NRAS activation occurs at the plasma membrane[29]. Therefore, it would be expected that NRAS would no longer be able to interact with its downstream effector proteins if it was not at the membrane. We treated both NRAS-driven and non-NRAS-driven melanoma cell lines with **1** as well as different controls to assess the differences in phosphorylated-AKT and phosphorylated-ERK. The phosphorylation of both of these proteins leads to activation of the oncogenic signaling pathways related to cancer cell growth and survival[30]. In the NRAS-driven melanoma cells, there was a dose-dependent decrease in p-AKT and p-ERK after 2-hour treatment with **1**, (Figure 2.5a,b). Single dose studies showed a significant decrease in p-AKT after 2-hour treatment with 10 μM of **1** compared to that of the untreated control, vehicle control, and compound **2** (Figure 2.6a,b and Figure 2.7a,c). A decrease in p-ERK after treatment with **1** was also observed. (Figure 2.6a,c and Figure 2.7e).

Next, we treated the Sk-Mel-28 BRAF-driven melanoma cell line with the same six treatment conditions to determine if the effects on downstream phosphorylation were dependent on NRAS palmitoylation in a non-NRAS-dependent cell line. This particular melanoma cell line served as a control because it is dependent on mutated BRAF V600E for cancer survival and has wildtype NRAS[31,32], suggesting that NRAS depalmitoylation should not affect its oncogenic downstream signaling. In the BRAF-mutated melanoma cell line, there was no significant decrease in either p-AKT or p-ERK after 2-hour treatment with 10 μM of **1**, while there was an expected significant decrease after treatment with 12 nM of the MEK inhibitor binimetinib[33,34] (Figure 2.6d-f). The total protein levels of β-actin, AKT, and ERK were similar for all treatment conditions

(Figure 2.7b,d,f), except for the ERK level in the binimetinib-treated BRAF-mutated melanoma cells. This particular ERK level was much higher than the rest of the treatments, which could be due to feedback loop activation when MEK is blocked by binimetinib[33]. These results confirmed that compound **1** causes an inhibition of downstream RAS signaling by the depalmitoylation of NRAS in an NRAS-dependent cell line compared to a non-NRAS-dependent cell line.

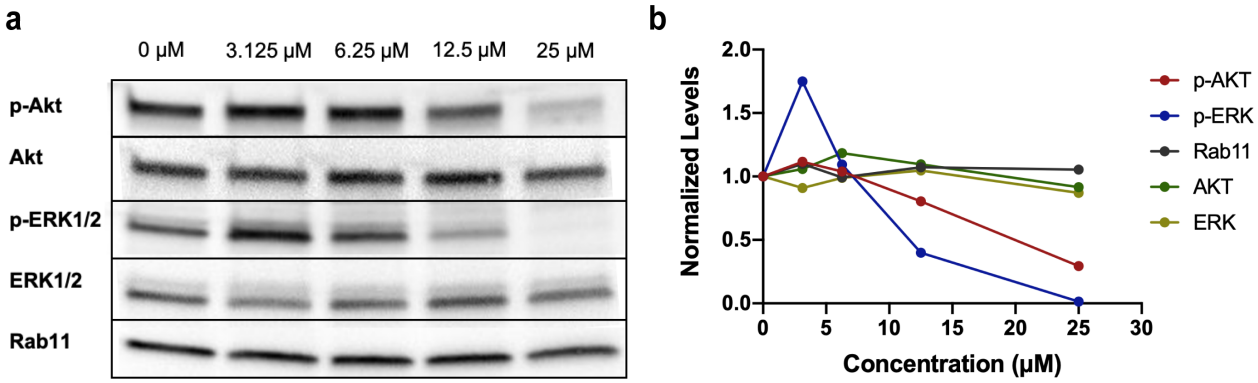

Figure 2.5 C8 Alkyl Cysteine Inhibits Oncogenic RAS Signaling in NRAS-Mutated Melanoma Cells in a Dose-Dependent Manner. **(a)** Western blot of increasing concentrations of C8 alkyl cysteine (**1**) in the WM3000 melanoma cell line with the NRAS Q61R mutation. **(b)** Western blot lanes for p-AKT, p-ERK, Rab11, AKT, and ERK were analyzed and quantified using ImageJ. Each dose treatment was normalized to the 0 μM control.

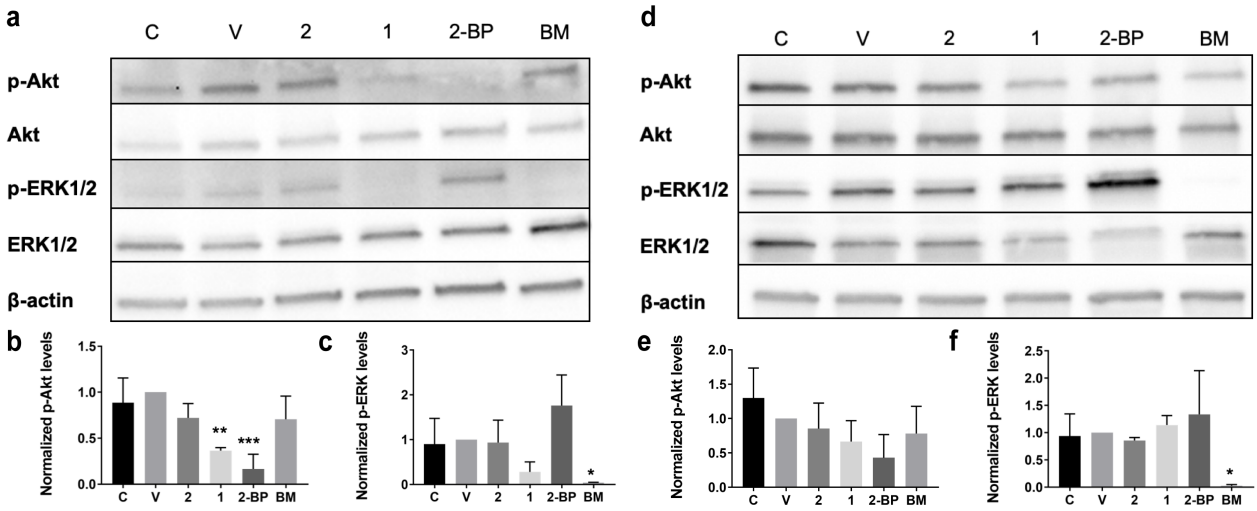

Figure 2.6 C8 Alkyl Cysteine Inhibits Oncogenic RAS Signaling in NRAS-Mutated Melanoma Cells Compared to BRAF-Mutated Melanoma Cells. **(a)** Western blot of six different treatment conditions in the WM3000 melanoma cell line with the NRAS Q61R mutation. Treatment conditions include the untreated control (C), vehicle control (20 μM TCEP in DMSO) (V), 10 μM C8 alkyl serine (**2**), 10 μM C8 alkyl cysteine (**1**), 10 μM 2-bromopalmitate (2-BP), and 12 nM binimetinib (BM). **(b,c)** Western blot lanes for p-AKT and p-ERK were analyzed and quantified using ImageJ. Each treatment condition was normalized to the vehicle control. Results are the mean ± s.d. of three independent experiments. *$p \leq 0.05$, **$p \leq 0.005$, ***$p \leq 0.0005$ (one-way ANOVA). **(d)** Western blot of the six different treatment conditions in the Sk-Mel-28 melanoma cell line with the BRAF V600E mutation. **(e,f)** Western blot lanes for p-AKT and p-ERK were analyzed and quantified using ImageJ. Each treatment condition was normalized to the vehicle control. Results are the mean ± s.d. of three independent experiments. *$p \leq 0.05$ (one-way ANOVA).

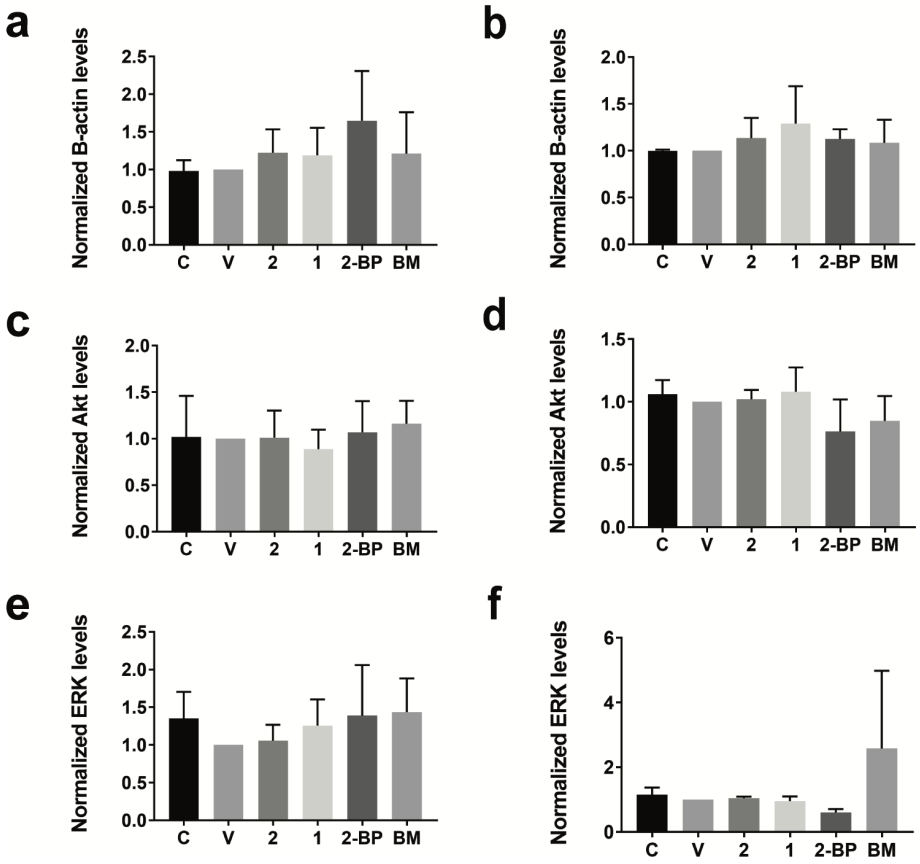

Figure 2.7 Western Blot Protein Levels in NRAS-Mutated Melanoma vs. BRAF-Mutated Melanoma. Treatment conditions include the untreated control (C), vehicle control (20 μM TCEP in DMSO) (V), 10 μM C8 alkyl serine (**2**), 10 μM C8 alkyl cysteine (**1**), 10 μM 2-bromopalmitate (2-BP), and 12 nM binimetinib (BM). There was no significant difference in β-actin levels in the **(a)** WM3000 NRAS-mutated melanoma cells or the **(b)** Sk-Mel-28 BRAF-mutated melanoma cells. There was no significant difference in total AKT levels in the **(c)** WM3000 NRAS-mutated melanoma cells or the **(d)** Sk-Mel-28 BRAF-mutated melanoma cells. There was no significant difference in total ERK levels in the **(e)** WM3000 NRAS-mutated melanoma cells or the **(f)** Sk-Mel-28 BRAF-mutated melanoma cells, excluding the MEK inhibitor binimetinib. Western blot lanes for all protein levels were analyzed and quantified using ImageJ. Each treatment condition was normalized to the vehicle control. Results are the mean ± s.d. of three independent experiments (one-way ANOVA).

2.3.4 Reduction of Cell Viability in NRAS-Driven Melanoma

High levels of p-AKT and p-ERK are associated with an upregulation of cell growth and survival pathways in cancer[1,30]. Since we determined that **1** inhibits oncogenic RAS signaling by decreasing p-AKT and p-ERK, we wanted to study the direct effects of the depalmitoylating compound on cell viability. Although our amphiphilic compound is expected to depalmitoylate multiple membrane-bound proteins[21], we expected that the depalmitoylation of NRAS would have the most significant effects on cell viability of NRAS-driven cell lines because they are dependent on NRAS for survival. In order to assess the importance of AMD chemical structure on growth inhibition activity, both NRAS-dependent and BRAF-dependent melanoma cell lines were treated with a variety of alkyl cysteine derivatives that had different chain lengths (Figure 2.8 and Figure 2.9). We determined that compound **1** was the most potent inhibitor of NRAS-mutated melanoma cell viability compared to the other lipid compounds (**2**–**6**), which could be due to the appropriate balance in hydrophobicity and hydrophilicity in the chemical structure and alkyl chain length of **1** (Figure 2.10a). This balance would allow compound **1** to have enough solubility for transmembrane permeability and amphiphilicity to insert itself into the membrane. Additionally, **1** was more selective for inhibiting NRAS-mutated melanoma viability vs. BRAF-mutated melanoma viability compared to **4**, which was the only other derivative that had an effect on cell viability of the NRAS-mutated melanoma cell line (Figure 2.10a-c).

Next, the WM3000 and Sk-Mel-2 NRAS-mutated human melanoma cell lines as well as the control Sk-Mel-28 BRAF-mutated human melanoma cell line were all treated with **1** at increasing concentrations of 0, 3.125, 6.25, 12.5, 25, and 50 μM for 24 hours. We found that **1** had over 8-fold more inhibitory activity in NRAS-mutant versus non-NRAS-mutant melanoma cells, with an inhibitory concentration of 50% (IC_{50}) of 9 μM in the WM3000 NRAS-mutated melanoma

cell line and 72 μM in the Sk-Mel-28 BRAF-mutated melanoma cell line (Figure 2.11a). There was similarly high potency in Sk-Mel-2 melanoma cell line, which showed an IC_{50} of 15 μM. The dose-dependent decrease in cell viability correlated well with the dose-dependent decrease in the palmitoylation of NRAS (Figure 2.1c and Figure 2.11a). These results support that **1** causes a reduction in NRAS palmitoylation leading to a decrease in NRAS-mutated melanoma cell viability.

To determine if the inhibitory effects of compound **1** were mediated by the release of NRAS from the plasma membrane, a cell viability rescue experiment was conducted using a fusion construct of NRAS(Q61R) with its C-terminal HVR replaced with the KRAS4b HVR (Figure 2.11b). The KRAS4b HVR anchors RAS to the plasma membrane via a polylysine motif instead of S-palmitoylation, and its localization is not affected by AMD[21]. Furthermore, while NRAS is dependent on S-palmitoylation for cell growth and survival[26,27], KRAS4b is not[13]. The original WM3000 NRAS(Q61R) melanoma cell line and the generated fusion WM3000 NRAS(Q61R)-KRAS4bHVR melanoma cell line both were treated with increasing concentrations of **1** for 24 hours. The IC_{50} of **1** was 9 μM in the WM3000 NRAS-mutated melanoma cell line and 16 μM in the stable WM3000 NRAS(Q61R)-KRAS4bHVR melanoma cell line (Figure 2.11c). Almost twice the concentration of **1** was necessary to have a similar decrease in cell viability in the NRAS-KRAS4bHVR cell line compared to the original NRAS-mutated melanoma cell line. It is possible that since the NRAS-KRAS4bHVR cell line still has endogenous NRAS(Q61R) mutant protein, there could be a threshold at which the NRAS-KRAS4bHVR fusion protein is unable to completely rescue cell viability if endogenous NRAS(Q61R) mutant protein is targeted by **1**. However, these results support that the reduction in cell viability is mediated by the depalmitoylation and release of NRAS from the plasma membrane.

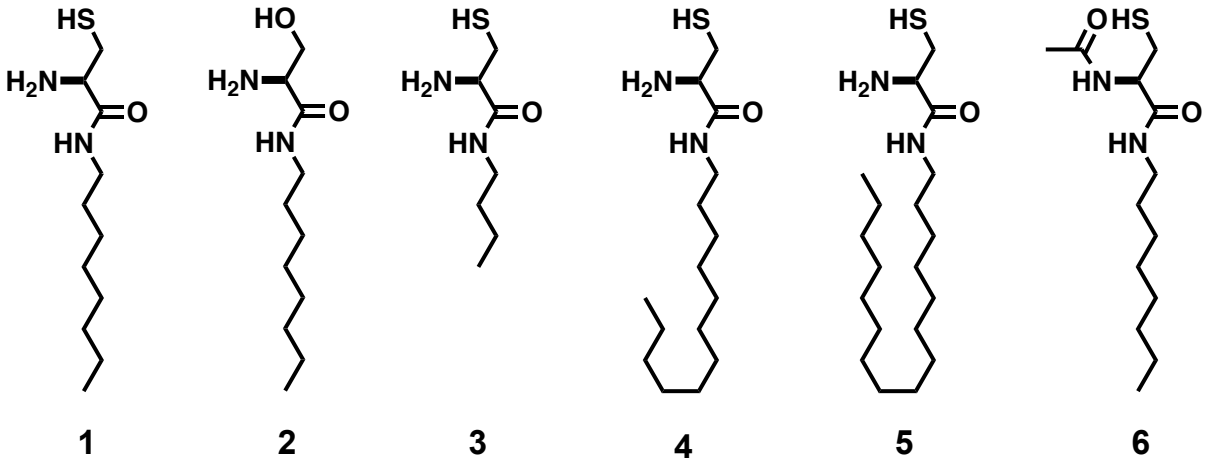

Figure 2.8 Chemical Structures of Alkyl Cysteine Derivatives and Controls. H_2N-*L*-Cys-Oct (**1**), H_2N-*L*-Ser-Oct (**2**), H_2N-*L*-Cys-But (**3**), H_2N-*L*-Cys-Dodec (**4**), H_2N-*L*-Cys-Hexad (**5**), and *N*-Ac-*L*-Cys-Oct (**6**).

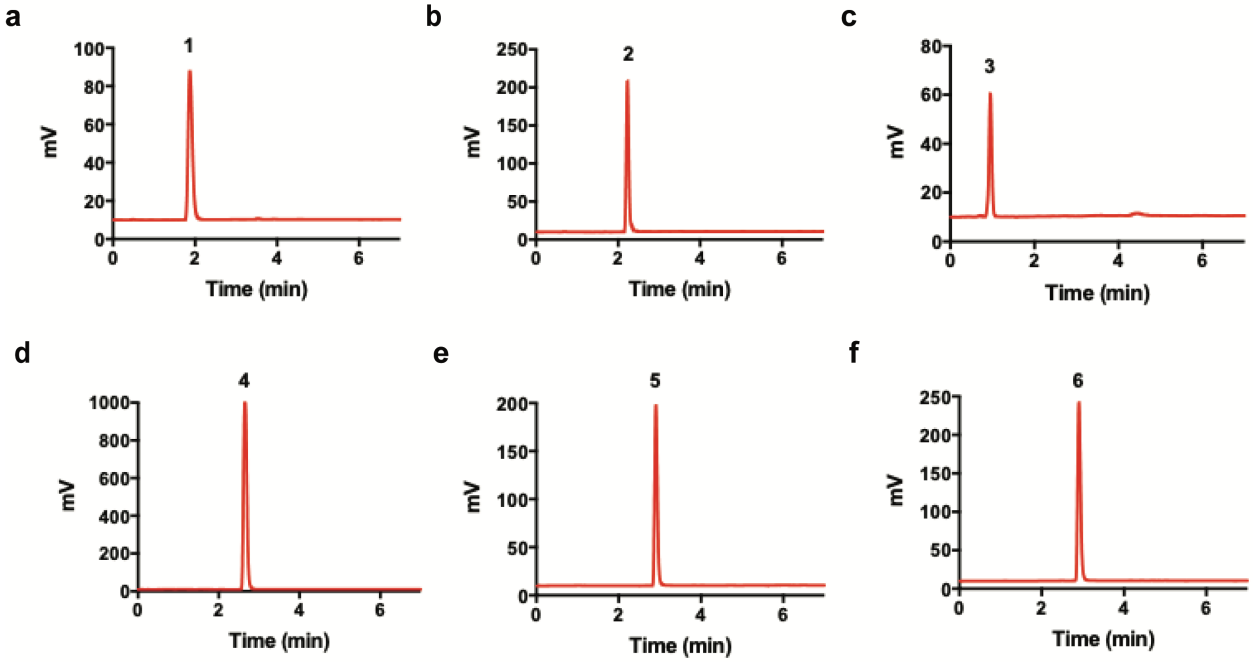

Figure 2.9 HPLC/ELSD Spectrum. **(a)** H_2N-*L*-Cys-Oct (**1**), **(b)** H_2N-*L*-Ser-Oct (**2**), **(c)** H_2N-*L*-Cys-But (**3**), **(d)** H_2N-*L*-Cys-Dodec (**4**), **(e)** H_2N-*L*-Cys-Hexadec (**5**), **(f)** *N*-Ac-*L*-Cys-Oct (**6**). Retention times (t_R) were verified by mass spectrometry.

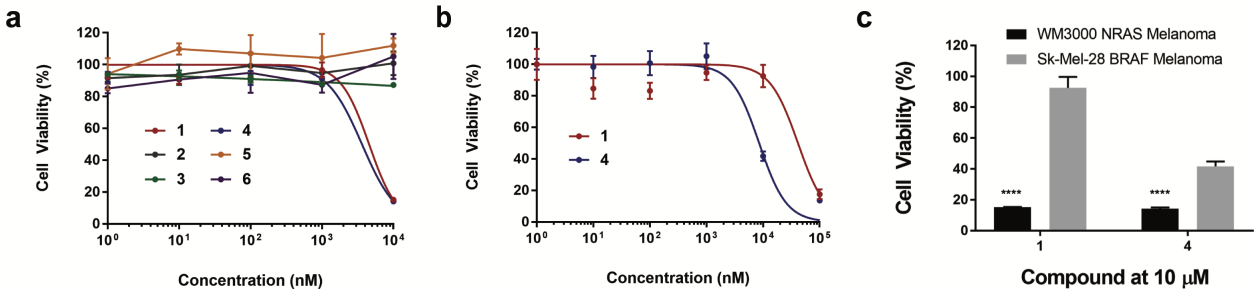

Figure 2.10 Cell Viability of Melanoma Cell Lines Treated with Alkyl Cysteine Derivatives and Controls. **(a)** WM3000 NRAS-mutated melanoma cells treated with six different compounds including C8 alkyl cysteine (**1**), C8 alkyl serine (**2**), C4 alkyl cysteine (**3**), C12 alkyl cysteine (**4**), C16 alkyl cysteine (**5**), and C8 acylated amine (**6**). **(b)** The control Sk-Mel-28 BRAF-mutated melanoma cells treated with two of the compounds (**1** and **4**) that had effects on the WM3000 melanoma cell line. **(c)** Comparison of treatment with 10 μM of either **1** or **4** between the WM3000 NRAS-mutated melanoma cell line and Sk-Mel-28 BRAF-mutated melanoma cell line from **(a)** and **(b)**. Results are the mean ± s.d. of three experiments. ****p ≤ 0.0001 (two-way ANOVA, multiple comparisons).

Figure 2.11 C8 Alkyl Cysteine Preferentially Reduces Cell Viability in NRAS-Driven versus BRAF-Driven Melanoma. **(a)** A WST-1 assay was used to assess the cell viability of NRAS-mutated melanoma cell lines (WM3000 and Sk-Mel-2) vs. a BRAF-mutated melanoma cell line (Sk-Mel-28) after 24-hour incubation with increasing concentrations of C8 alkyl cysteine. Results are the mean ± s.d. of three independent experiments. Each row (concentration) was analyzed individually, without assuming a consistent SD. **p ≤ 0.01, ***p ≤ 0.001 (multiple t-tests). **(b)** The last 24 amino acids of the hypervariable region (HVR) of NRAS and KRAS4b are marked in red. The final protein construct of the NRAS-KRAS4bHVR fusion that was used for experimentation is at the bottom. **(c)** A WST-1 assay was used to assess the cell viability of the original WM3000 NRAS-mutated melanoma cell line and the WM3000 NRAS-mutated melanoma cell line with KRAS4b HVR replacing the original NRAS C-terminal HVR. Both cell lines were treated with increasing concentrations of C8 alkyl cysteine for 24 hours. Results are the mean ± s.d. of three independent experiments. Each row (concentration) was analyzed individually, without assuming a consistent SD. ***p ≤ 0.001 (multiple t-tests).

2.3.5 Apoptosis Induction in NRAS-Driven Melanoma Tumors

Having demonstrated the inhibitory effect of NRAS depalmitoylation *in vitro*, we sought to explore the activity of **1** in melanoma xenograft mouse models. Mice implanted with either WM3000 (NRAS-mutant) or Sk-Mel-28 (BRAF-mutant) melanoma cells were intratumorally injected with either 50 mg/kg compound **1** or vehicle control (Figure 2.12a).

To evaluate tumor cell survival, apoptosis, and p-ERK activity, consecutive tumor sections were stained for Ki-67, cleaved-caspase-3 (CC3), and p-ERK 24-hours after treatment. The Ki-67 nuclear antigen is highly expressed in cells undergoing active phases of the cell cycle (G1, S, G2, and M) but is absent in the G0 phase when the cells are in a quiescent state[35]. Hence, the expression of Ki-67 is strongly correlated with cell proliferation. We observed a decrease in Ki-67 in the NRAS tumors treated with compound **1** compared to vehicle control, while the BRAF tumors treated with **1** and vehicle control exhibited similar levels of Ki-67 staining (Figure 2.12b).

Intratumoral injection of compound **1** in NRAS-mutated tumors showed strong staining for CC3 activity, which is a common and reliable marker to assess apoptosis in various tissues[36,37], compared to vehicle control, and minimal CC3 activity was observed in BRAF-mutated tumors. This confirmed that compound **1** was capable of inducing programmed cell death in NRAS, but not BRAF-mutated tumors (Figure 2.12b).

Finally, to determine if intratumoral injection of compound **1** can downregulate RAS signaling in NRAS tumors, tissue sections were stained for p-ERK activity. We observed p-ERK staining in the BRAF-mutated tumors treated with **1** as well as vehicle controls of both the BRAF and NRAS-mutated tumors, but there was much less p-ERK staining in the NRAS-mutated tumors treated with **1** (Figure 2.12b). These results were in line with our *in vitro* data showing a downregulation of the RAS signaling pathway in an NRAS-mutated melanoma cell line upon

treatment with **1** (Figure 2.6a-c). Together, these studies demonstrated that compound **1** was able to achieve tumor cell killing and downregulate p-ERK signaling in NRAS-driven melanoma tumors, but not in BRAF-driven melanoma tumors.

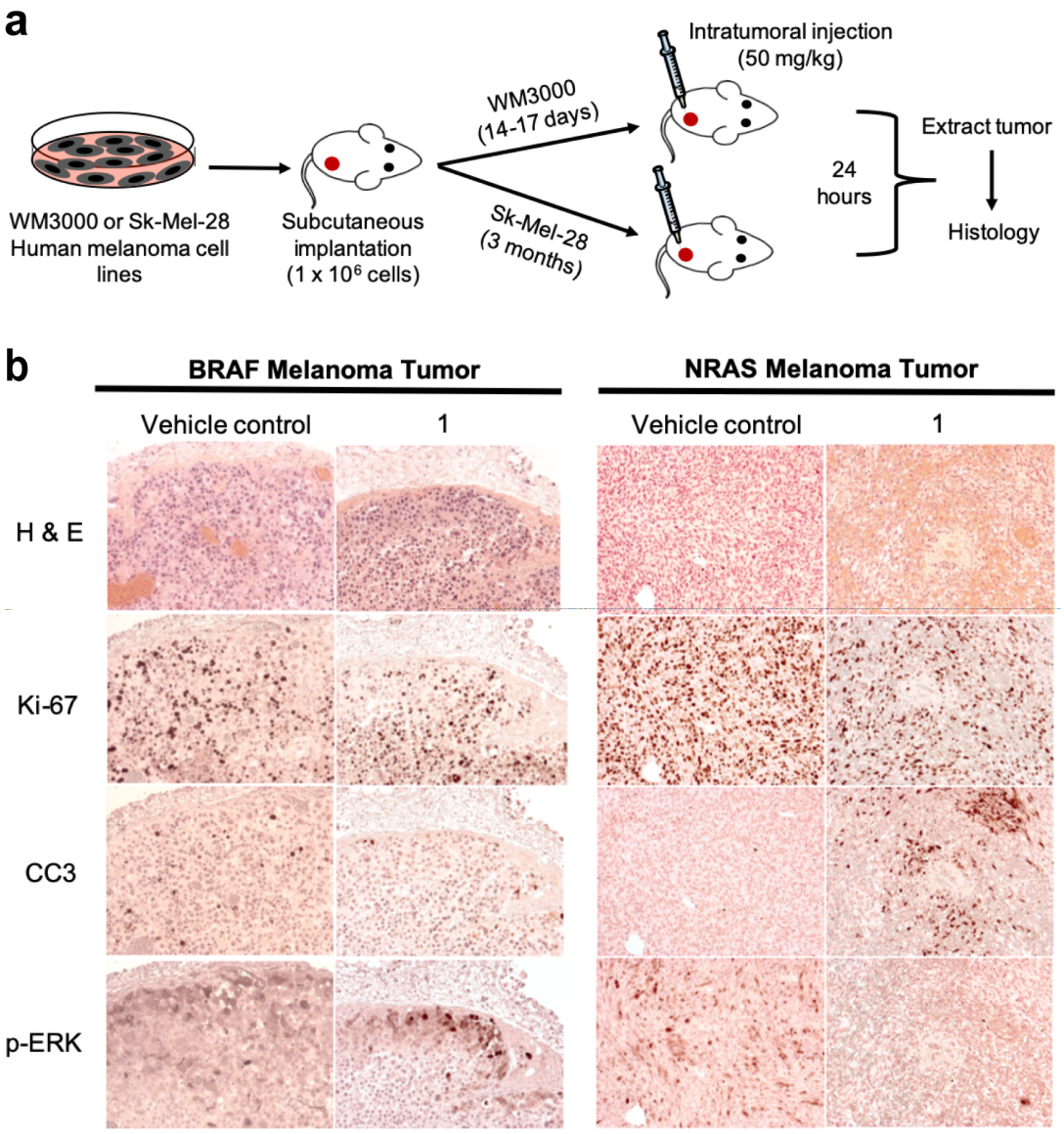

Figure 2.12 C8 Alkyl Cysteine Reduces Proliferation and Induces Apoptosis in NRAS-Driven versus BRAF-Driven Melanoma Tumors. **(a)** Schematic and timeline of *in vivo* subcutaneous melanoma xenograft implantation and intratumoral (IT) treatments. **(b)** Histology was performed for BRAF-mutated melanoma tumors (Sk-Mel-28) and NRAS-mutated melanoma tumors (WM3000) for both vehicle control (123.51 mg/kg TCEP in saline) and C8 alkyl cysteine (**1**) treatment groups. Consecutive tissue sections were stained with hematoxylin and eosin (H&E) for tumor cell morphology, anti-Ki-67 for cell proliferation, anti-cleaved caspase-3 (CC3) for cell apoptosis, and anti-phosphorylation of ERK (p-ERK) for RAS signaling.

2.3.6 Tumor Growth Decrease in NRAS Melanoma Xenografts

After confirming the ability of compound **1** to induce cell death in the NRAS-mutated melanoma tumors, we proceeded to examine the effectiveness of treatment with **1** in the NRAS-mutant tumor bearing mice by intraperitoneal (IP) administration. The xenograft mice were randomized into either compound **1 (**20 mg/kg) or vehicle control (49.40 mg/kg) treatment groups for a 7-day study (Figure 2.13a). Daily treatment with **1** resulted in a significant decrease in tumor growth compared to the vehicle control cohort (Figure 2.13b). Importantly, the body weight of the animals did not change over the course of treatment, suggesting that compound **1** was well tolerated at this treatment regimen (Figure 2.13c).

Drug-induced hepatotoxicity is a frequent cause of liver injury with the use of many cancer therapies[38]. To determine if **1** caused liver toxicity in the xenograft mice, alanine aminotransferase (ALT) enzyme was measured from the serum. ALT is found mainly in the liver and kidney, and normally at low levels in the blood. However, when the liver is damaged ALT is released resulting in high levels in the bloodstream. ALT levels after IP treatment were approximately 60 mU/mL for **1** and 90 mU/ml for vehicle control (Figure 2.13d). These levels were not significantly different from one another and within the normal range for mice, which is between 26–126 U/L[39]. This strongly suggested that compound **1** did not induce liver toxicity in the mice.

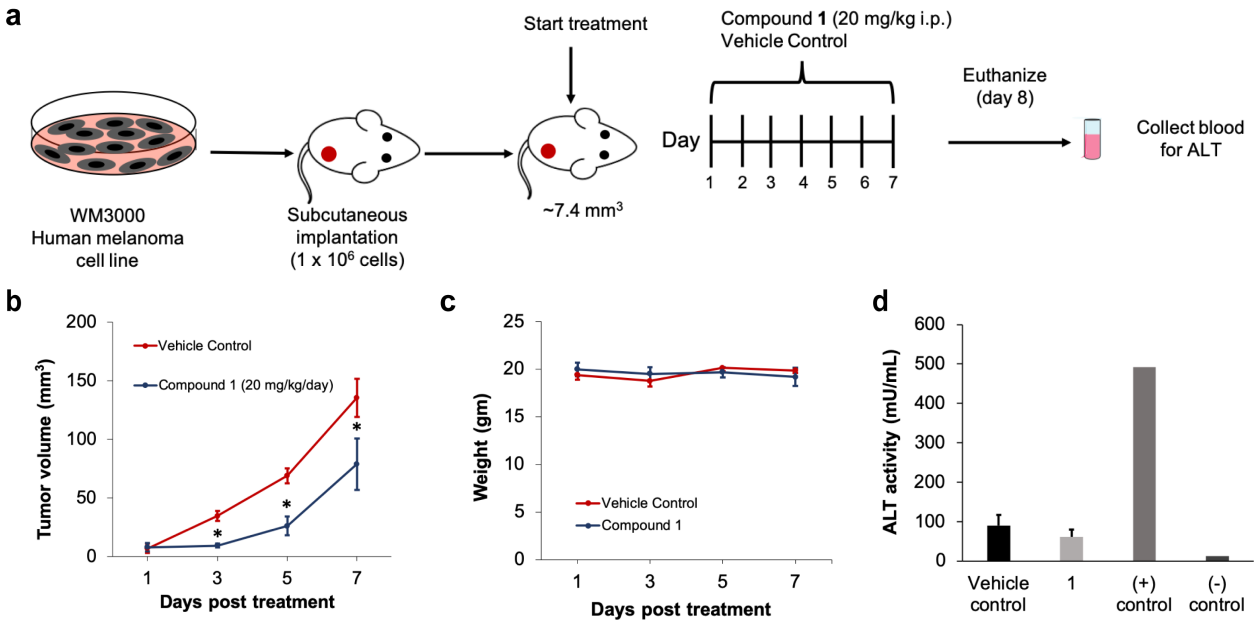

Figure 2.13 C8 Alkyl Cysteine Causes a Decrease in Tumor Growth in NRAS-Mutated Melanoma Xenograft Mice. **(a)** Schematic and timeline of *in vivo* melanoma xenograft intraperitoneal (IP) treatments. **(b)** WM3000 NRAS-mutated human melanoma xenograft mice were IP injected with either 20 mg/kg/day of **1** or 49.40 mg/kg/day (2 molar equivalents) of vehicle control. Tumor volume was measured every other day for one week for both treatment groups. Results are the mean ± SEM with n = 6. *p ≤ 0.05 (unpaired, two-tailed Student's *t* test). **(c)** Animal weight was measured every other day for the duration of the IP treatments. **(d)** Liver toxicity was analyzed by assessing the alanine aminotransferase (ALT) activity in the blood samples of the xenograft mice in both treatment groups. The conditions included 49.40 mg/kg/day of vehicle control, 20 mg/kg/day of C8 alkyl cysteine (**1**), ALT enzyme assay positive control (+), and untreated mouse negative control (-).

2.4 Discussion

NRAS GTPase has been deemed as an undruggable protein because of the challenging nature of targeting its shallow binding pockets. Directly targeting the S-palmitoylation modification on the C-terminal HVR of NRAS using a chemoselective approach can be applied as a unique inhibition strategy. It has been well documented through *in vitro* and *in vivo* studies that NRAS palmitoylation is required for its cancer signaling activity[26,27]. Taking this into account, our depalmitoylation strategy can be used to target NRAS palmitoylation and inhibit its oncogenic signaling capabilities in the context of NRAS-driven cancers.

We have determined that our depalmitoylating compound, C8 alkyl cysteine (**1**), causes delocalization of NRAS from the plasma membrane by the mechanism of depalmitoylation. Additionally, **1** inhibits downstream signaling associated with cancer cell growth and survival pathways in NRAS-mutated melanoma cells (Figure 2.14). Specifically, it causes a decrease in p-AKT and p-ERK in an NRAS-driven cell line but not in a BRAF-driven cell line that is not dependent on NRAS signaling. Accordingly, **1** causes an inhibitory effect on cell viability in multiple NRAS-mutated melanoma cell lines, which is rescued by addition of an NRAS mutant with its HVR replaced with the non-palmitoylated HVR of KRAS4b. However, it is important to note that there is not a complete rescue in cell viability of the NRAS-KRAS4bHVR cell line. A possible explanation for this result is that there is still endogenous mutant NRAS that is depalmitoylated by **1**, which may contribute to the partial rescuing capability of the NRAS-KRAS4bHVR fusion protein up until a certain concentration. In a xenograft mouse model, tumor histology confirmed that **1** was able to induce apoptosis after intratumoral injection in NRAS-mutated melanoma tumors, but not BRAF-mutated melanoma tumors. We were also able to detect a downregulation of p-ERK signaling in the NRAS-dependent melanoma tumors with direct

intratumoral injection. Furthermore, we observed a significant decrease in tumor growth in NRAS-mutated melanoma xenograft mice treated with **1** compared to the vehicle control, with no detectable liver toxicity. Taken together, these results indicate that compound **1** can inhibit NRAS function *in vitro* and *in vivo*.

This unique depalmitoylation approach overcomes the issues associated with designing small molecules to bind the active site of NRAS and provides a direct method to inhibit its function by targeting the S-palmitoylation post-translational modification. A depalmitoylation-based strategy has the potential to be transformative for the treatment of melanoma as well as other cancers with high rates of NRAS-mutations, such as leukemias and lymphomas. Our ongoing work includes enhancing the selectivity of the amphiphile-mediated depalmitoylating compounds. We plan to use appropriate large-scale capture techniques and proteomic methods for analyzing the palmitoylated proteins that are targeted by these compounds[40,41]. In addition, we plan to explore the direct relationship between NRAS palmitoylation and total Ras-GTP levels in future studies[42,43]. With further optimization of the selectivity and pharmacokinetics, amphiphile-mediated depalmitoylation could become a strategy to uncover novel lead compounds that can be adapted to generate inhibitors of several other S-palmitoylated drug targets across a wide range of disease indications.

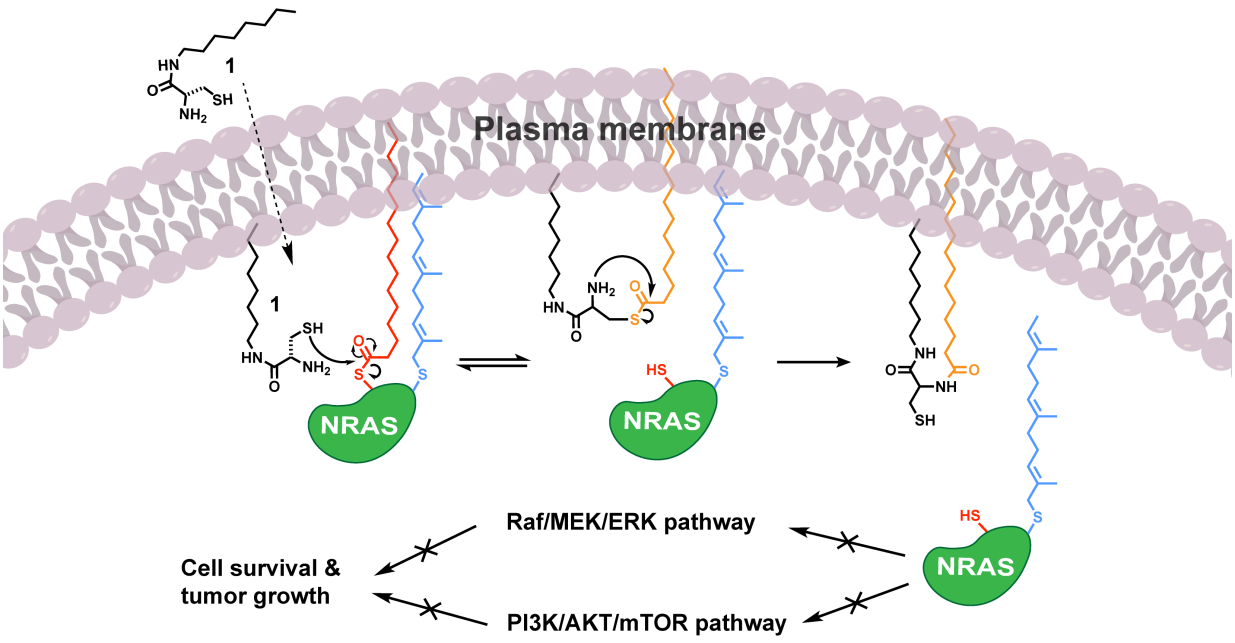

Figure 2.14 Schematic Representation of NRAS Depalmitoylation and Downstream Inhibition by C8 Alkyl Cysteine.

2.5 Materials and Methods

2.5.1 Cell Culture

The WM3000 (NRAS Q61R mutation) and WM2013 (NRAS Q61K mutation) melanoma cell lines were purchased from Rockland Immunochemicals and cultured in Tumor Specialization Media according to the melanoma cell culture protocol. The Tumor Specialization Media was prepared in the laboratory by mixing 400 mL of MCDB 153 (Sigma-Aldrich), 100 mL of Leibovitz's L-15 (Life Technologies), 10 mL of heat-inactivated FBS (Omega Scientific), and 0.42 mL of $CaCl_2$. The Sk-Mel-2 (NRAS Q61K mutation) melanoma cell line was purchased from ATCC and cultured in EMEM with 10% FBS. The Sk-Mel-28 (BRAF V600E mutation) melanoma cell line was generously provided by Dr. Silvio Gutkind at the UCSD Moores Cancer Center and cultured in EMEM with 10% FBS. HeLa S3 cells were obtained from ATCC. Cells were maintained in DMEM supplemented with 10% fetal bovine serum (FBS) at 37 ºC, 5% CO_2. The DMEM growth media was purchased from Life Technologies, and the EMEM growth media was purchased from Thermo Fisher Scientific.

2.5.2 Plasmid Construction and Cloning

Hs.NRAS was a gift from Dominic Esposito (Addgene plasmid # 83173) and mEGFP-C1 was a gift from Michael Davidson (Addgene plasmid # 54759). The primers 5'-CTT-CGA-ATT-CTG-CAG-TCG-ACA-TGC-CAA-CTT-TGT-ACA-AAA-AAG-3' (NRAS-fwd) and 5'-GAT-CCC-GGG-CCC-GCG-GTA-CCT-TAC-ATC-ACC-ACA-CAT-GG-3' (NRAS-rev) were used for PCR amplification of the NRAS insert and the primers 5'-CTT-TTT-TGT-ACA-AAG-TTG-GCA-TGT-CGA-CTG-CAG-AAT-TCG-AAG-3' (mEGFP-C1-fwd) and 5'-CCA-TGT-GTG-GTG-ATG-TAA-GGT-ACC-GCG-GGC-CCG-GGA-TC-3' (mEGFP-C1-rev) were used for PCR amplification of the mEGFP-C1 vector, which were ligated using Gibson assembly (New England

Biolabs), and cloned in DH5α competent *E. coli* cells to produce the final EGFP-NRAS plasmid. The final construct was sequenced by Eton Bioscience to verify its identity, and the SnapGene software was used for sequence alignment. The final plasmid used for transfection was prepared using a plasmid maxiprep kit (EZgene).

pCMV(CAT)T7-SB100 was a gift from Zsuzsanna Izsvak (Addgene plasmid # 34879)[44]. pSBbi-Pur was a gift from Eric Kowarz (Addgene plasmid # 60523)[45]. pSBbi-Pur-EGFP-NRAS was constructed using NEBuilder HiFi Assembly (New England Biolabs). The vector pSBbi-Pur was linearized using SfiI and inserts were prepared by PCR amplification of EGFP-NRAS with the following primers: 5'-CTA-CCC-CAA-GCT-GGC-CTC-TGA-GGC-CAT-GGT-GAG-CAA-GGG-CGA-G-3' (EGFP-NRAS-fwd) and 5'-ATC-CCC-AAG-CTT-GGC-CTG-ACA-GGC-CTT-ACA-TCA-CCA-CAC-ATG-GCA-ATC-3' (EGFP-NRAS-rev). The final construct was sequenced by Eton Bioscience to verify its identity, and the SnapGene software was used for sequence alignment. The final plasmid used for transfection was prepared using a plasmid maxiprep kit (EZgene).

pSBbi-RP was a gift from Eric Kowarz (Addgene plasmid # 60513)[45]. The primers 5'-AGC-TGG-CCT-CTG-AGG-CCA-CCA-TGC-CAA-CTT-TGT-ACA-A-3' (NRAS-Q61R-forward) and 5'-AGC-TTG-GCC-TGA-CAG-GCC-ATT-ACA-TAA-TTA-CAC-ACT-TTG-TCT-T-3' (NRAS-Q61R-reverse), which include the SfiI restriction site, were used for PCR amplification of the NRAS(Q61R)-KRAS4bHVR insert out of a previously created lentiviral transfer plasmid (Supplementary Figure 8). Restriction enzyme digest with SfiI was done for the NRAS(Q61R)-KRAS4bHVR insert and the pSBbi-RP vector. The two samples – insert and vector – were run on an 0.8% agarose gel and extracted using the QIAquick Gel Extraction Kit (Qiagen). The NRAS(Q61R)-KRAS4bHVR insert and pSBbi-RP vector were ligated using the T4 DNA Ligase

ligation protocol and transformed into NEB stable DH5α competent *E. coli* cells. The final construct was sequenced by Eton Bioscience to verify its identity, and the SnapGene software was used for sequence alignment.

2.5.3 Generation of Stable Cell Lines

HeLa S3 cells stably expressing EGFP-NRAS were established using the Sleeping Beauty transposon system with the improved transposase SB100X[44,45]. HeLa S3 cells grown in a 6-well plate were transfected with pSBbi-Pur-EGFP-NRAS and pCMV(CAT)T7-SB100 at a 20:1 ratio [1.5 μg total DNA/well] using Lipofectamine 2000 reagent (Thermo Fisher Scientific) [3 uL/well] according to the manufacturer's protocol. 2 days after transfection, cells were expanded into 6 cm plates with selection media (DMEM; 10% FBS; 2 μg/mL puromycin). Cells were passaged under selection conditions for 2 weeks before experimental use.

A stable transgenic melanoma cell line with the NRAS(Q61R)-KRAS4bHVR was generated using the Sleeping Beauty transposons system[44,45]. The final NRAS(Q61R)-KRAS4bHVR construct was co-transfected with low amounts of the transposase SB100X into the WM3000 human melanoma cell line on 6-well plates using Lipofectamine 2000 reagent (Thermo Fisher Scientific) according to the manufacturer's protocol in Opti-MEM reduced serum medium (Life Technologies). After 2 days, the transfected cells in each well were split onto new 6-well plates for selection with ranging concentrations of puromycin (0 μg/mL, 0.5 μg/mL, 1 μg/mL, and 2 μg/mL) to determine the puromycin kill curve and only select for melanoma cells that were stably transfected with the Sleeping Beauty NRAS(Q61R)-KRAS4bHVR construct.

2.5.4 Live-Cell Imaging of Stable HeLa S3 Cells

HeLa S3 cells stably expressing EGFP-NRAS were plated at 80,000 cells/well in an 8-well Lab-Tek II chamber slide (Thermo Fisher Scientific) and allowed to adhere overnight. The media was

exchanged for Opti-MEM reduced serum medium (Life Technologies) before live-cell imaging with different treatment conditions. 100 mM stock solutions of compounds **1** and **2** were prepared by dissolving the solid compounds in DMSO containing 200 mM tris(2-carboxyethyl)phosphine hydrochloride (TCEP) as a preservative. 100 mM stock solutions of 2-BP was prepared by dissolving the solid compound in DMSO. From these stocks, solutions of 40 μM **1** or **2** (with 80 μM TCEP) or 40 μM 2-BP were prepared in Opti-MEM media. The diluted solutions were added to the indicated final concentration in Opti-MEM within individual wells of the chamber slide right before imaging. The cells were imaged while maintaining 37 ºC, 5% CO_2 in the incubation chamber.

2.5.5 Microscopy

Imaging was performed on an Axio Observer Z1 inverted microscope (Carl Zeiss Microscopy Gmb, Germany) with Yokogawa CSU-X1 spinning disk confocal unit using a 63x, 1.4 NA oil immersion or 20x, 0.8 NA objective to an ORCA-Flash4.0 V2 Digital CMOS camera (Hamamatsu, Japan). For live cell imaging, an incubation chamber with temperature and CO_2 controllers (Okolab Incubation System, H301-K-FRAME stage top chamber) was utilized. Fluorophores were excited with diode lasers (488 nm; 561 nm). Images were acquired using Zen Blue software (Carl Zeiss) and processed using Image J.

2.5.6 S-palmitoylation Acyl-RAC Assay

WM3000 melanoma cells were plated at 2,450,000 cells/dish in 10 cm tissue culture dishes (Genesee Scientific) and allowed to adhere overnight. 100 mM stock solutions of compounds **1** and **2** were prepared by dissolving the solid compounds in DMSO containing 200 mM TCEP as a preservative. 100 mM stock solution of vehicle control was prepared by dissolving TCEP in DMSO. 100 mM stock solution of 2-BP was prepared by dissolving the solid compound in DMSO.

From these stocks, solutions of 10 μM **1** or **2** (with 20 μM TCEP), 20 μM vehicle/TCEP, or 10 μM 2-BP were diluted in 6.13 mL of Opti-MEM media and added to the cells. Cells were then incubated at 37 ºC for 2 hours, media was removed, and cells were washed with 1 mL of HBSS. Cells were detached using a cell scraper after the combined thiol blocking and cell lysis steps of the CAPTUREome S-Palmitoylated Protein Kit (Badrilla, UK) according to the manufacturer's protocol. Input fractions (IF) that consisted of the total proteins and bound fractions (BF) that consisted of the resin-captured S-palmitoylated proteins were ran on a 4–20% SDS-PAGE gel. All of the IF and BF samples were analyzed using western blotting, following the immunoblot protocol below, using the anti-NRAS primary antibody (ab227658) (Abcam). Western blot lanes were analyzed and quantified using ImageJ. Ratios of BF to IF for each of the treatment conditions were calculated and normalized to the control to determine the amount of S-palmitoylated NRAS in each sample. Additionally, BF samples were analyzed using silver staining, following the manufacturer's protocol (Thermo Fisher Scientific).

2.5.7 Western Blots

Cell lysates were prepared from confluent WM3000 and Sk-Mel-28 melanoma cell lines that were treated with six different conditions in Opti-MEM media for 2 hours. Stock solutions of compounds were prepared in DMSO at a concentration of 100 mM as before and diluted to the final concentrations. 10 mM stock solution of binimetinib (BM) was prepared by dissolving the solid compound in DMSO, and a final solution of 12 nM concentration (IC_{50} of BM[46]) was diluted in Opti-MEM media before adding to the cells. After a 2-hour incubation, cells were washed with 1X HBSS and lysed using 0.6 mL of complete RIPA per subconfluent monolayer on a 100 mm cell culture dish. Immediately prior to lysing the cells, 10 μL PMSF solution, 10 μL sodium orthovanadate solution, and 10 μL protease inhibitor cocktail solution per mL of 1X RIPA Lysis

buffer were combined to prepare complete RIPA solution (Santa Cruz Biotechnology). The dishes were placed on a shaker for 10 minutes at room temperature. The cell lysates were scraped off the dishes using cell scrapers and pipetted into separate Eppendorf tubes. The tubes were centrifuged at 14,000 rpm for 10 minutes at 4°C. The supernatant was transferred into new tubes and placed on ice. The reducing agent compatible BCA protein assay kit (Thermo Fisher Scientific) was used to measure protein concentration. Total protein in 1X Laemmli buffer with 10% 2-mercaptoethanol was separated by SDS/PAGE on a 4–20% gradient precast acrylamide gel for 30 minutes at 200 V, transferred to a PVDF membrane for 1 hour at 100 V, and blocked for 1 hour in 5% BSA. Membranes were incubated overnight at 4°C with primary antibodies. Horseradish peroxidase-conjugated anti-rabbit IgG (Cell Signaling) or anti-mouse IgG (Sigma) were used as secondary antibodies, and membranes were developed using enhanced chemiluminescence (Thermo Fisher Scientific). β-Actin (3700), p-AKT (4060), AKT (4691), p-ERK (4370), ERK (4695), Calnexin (2433), Flotillin-1 (3253), Flotillin-2 (3436), SNAP25 (5308), Gα(i) (5290), and Lyric/Metadherin (14065) primary antibodies were purchased from Cell Signaling Technology. Western blot lanes were analyzed using ImageJ software and normalized to the vehicle/TCEP control.

2.5.8 Cell Viability Assay

The melanoma cell lines were plated at 10,000 cells per well on 96-well plates in Opti-MEM medium. Stock solutions of compounds were prepared in DMSO as before at a concentration of 100 mM and diluted to the final concentrations. The cells were treated with different concentrations of compounds the following day and incubated for 24 hours. Cell viability was assessed using the WST-1 cell proliferation reagent (Sigma-Aldrich) following the manufacturer's instructions. After incubation for 1 hour with the WST-1 reagent, absorbance was measured at 450 nm using a plate reader.

2.5.9 Animal Model

All animal experiments performed in this study were approved and compliant with ethical regulations provided by the University of California San Diego Institutional Animal Care and Use Committee (IACUC). Six-week-old female Nu/Nu nude mice (088) purchased from Charles River Laboratories were given ad lib access to food and water. For subcutaneous implantation, 1 x 10^6 WM3000 or Sk-Mel-28 cells were spun down and resuspended in 50 ul of 1X PBS plus 50 ul of Matrigel [Mediatech Inc. (Corning)] and kept on ice until ready to use. Cells were implanted subcutaneously into the right flank of anesthetized mice using a 1 cc syringe. Tumor growth was monitored weekly until palpable, at which point a caliper was used and tumor volume was calculated by using the formula V = 1/2(Length x Width^2). For intratumoral injection (n=2), animals were anesthetized with ketamine:xylazine cocktail (17.5 mg/ml ketamine:2.5 mg/ml xylazine, at 0.1 ml/20 g body weight IP) and injected with 50 mg/kg compound 1 (mixed with 2 molar equivalents of TCEP) or with 123.51 mg/kg vehicle/TCEP control (2 molar equivalents) at 0.1 ml/10 g body weight. A volume of 20 μL was injected directly into the tumor in one-minute increments around the whole tumor. For intraperitoneal (IP) treatment, 20 mg/kg compound **1** (mixed with 2 molar equivalents of TCEP) or 49.40 mg/kg vehicle/TCEP control was administered daily for seven days. All compounds were reconstituted in sterile saline solution.

2.5.10 Histology and Immunohistochemistry

Tumors were resected and placed in 10 % formalin for 24 hours, then transferred to 70 % ethanol, paraffin-embedded and sectioned (4 μm thick). All slides were baked at 60 °C for 1 hour to deparaffinized. Once cool, slides were rehydrated through successive alcohols (Xylene 3min, 100% EtOH 3 min (2X), 95% EtOH 3min (2X), 70% EtOH 3 min (2X), diH_2O). Slides were then stained with hematoxylin and eosin (H & E). For immunohistochemistry, slides underwent antigen

retrieval by boiling in sodium citrate buffer pH 6.0 for 15 minutes and cooled at room temperature for 30–40 minutes. Pap pen was drawn around the tissue and blocked with 3% H_2O_2 in background punisher (Biocare, cat # BP974) for 10 min, then washed 5 min (2X) in 1X TBST. Slides were protein blocked again with background punisher for another 10 min. Slides were then incubated with cleaved caspase-3 primary antibody (rabbit, Cell Signaling, cat # 9661L, 1:1000), p-ERK primary antibody (rabbit, Cell Signaling cat # 4370, 1:400) in 2.5 % normal horse serum (Vector Labs cat # S-2012), or one drop of Ki67 primary antibody (rabbit, Diagnostic Biosystems, part # RMPD004) at room temperature for 1 hour. Slides were then washed in 1X TBST for 5 min (2X), incubated with anti-rabbit HRP polymer secondary antibody (Biocare, cat # RMR622) for 30 min at room temperature, washed in 1X TBST for 5 min (2X), developed with DAB (Vector Laboratories, cat # SK-4105) for 5 min, and then washed in ice cold diH_2O to stop the reaction. Slides were then dehydrated [50% EtOH, 70% EtOH 3 min (2X), 95% EtOH 3 min (2X), 100% EtOH 3 min (2X), xylene 3 min (2X)] and mount in permount mounting medium (Fisher Scientific, part # SP15500).

2.5.11 Alanine Aminotransferase (ALT) Activity

Serum samples were collected at the end of the study and assayed for ALT levels using the Alanine Aminotransferase Activity Assay Kit according to manufacturer protocol (Sigma-Aldrich, Cat # MAK052).

2.6 Synthesis of Alkyl Reagents

2.6.1 General Considerations for Synthesis

Commercially available *N*-Boc-*L*-Cys(Trt)-OH, *N*-Ac-*L*-Cys(Trt)-OH, *N*-Boc-*L*-Cys-OH, *N*-Boc-*L*-Ser(^{t}Bu)-OH, O-(7-azabenzotriazol-1-yl)-1,1,3,3-tetramethyluronium hexafluoro-phosphate

(HATU), *N*,*N*-diisopropylethylamine (DIEA), butylamine, octylamine, dodecylamine, hexadecylamine, bromomethylacetate, sodium hydride (NaH), *N*,*N*-dimethylformamide (DMF), trifluoroacetic acid (TFA), triethylsilane (TES) and tris(2-carboxyethyl)phosphine hydrochloride (TCEP.HCl) were obtained from Sigma-Aldrich. Deuterated chloroform ($CDCl_3$) and methanol (CD_3OD) were obtained from Cambridge Isotope Laboratories. All reagents obtained from commercial suppliers were used without further purification unless otherwise noted. Analytical thin-layer chromatography was performed on E. Merck silica gel 60 F_{254} plates. Compounds, which were not UV active, were visualized by dipping the plates in a ninhydrin or potassium permanganate solution and heating. Silica gel flash chromatography was performed using E. Merck silica gel (type 60SDS, 230–400 mesh). Solvent mixtures for chromatography are reported as v/v ratios. HPLC analysis was carried out on an Eclipse Plus C8 analytical column with *Phase A*/*Phase B* gradients [*Phase A*: H_2O with 0.1% formic acid; *Phase B*: MeOH with 0.1% formic acid]. HPLC purification was carried out on Zorbax SB-C18 semipreparative column with *Phase A*/*Phase B* gradients [*Phase A*: H_2O with 0.1% formic acid; *Phase B*: MeOH with 0.1% formic acid]. Proton nuclear magnetic resonance (^{1}H NMR) spectra were recorded on a Varian VX-500 MHz or Jeol Delta ECA-500 MHz spectrometers, and were referenced relative to residual proton resonances in $CDCl_3$ (at δ 7.24 ppm) or CD_3OD (at δ 4.87 or 3.31 ppm). ^{1}H NMR splitting patterns are assigned as singlet (s), doublet (d), triplet (t), quartet (q) or pentuplet (p). All first-order splitting patterns were designated on the basis of the appearance of the multiplet. Splitting patterns that could not be readily interpreted are designated as multiplet (m) or broad (br). Carbon nuclear magnetic resonance (^{13}C NMR) spectra were recorded on a Varian VX-500 MHz or Jeol Delta ECA-500 MHz spectrometers, and were referenced relative to residual proton resonances in $CDCl_3$

(at δ 77.23 ppm) or CD_3OD (at δ 49.15 ppm). Electrospray Ionization-Time of Flight (ESI-TOF) spectra were obtained on an Agilent 6230 Accurate-Mass TOFMS mass spectrometer.

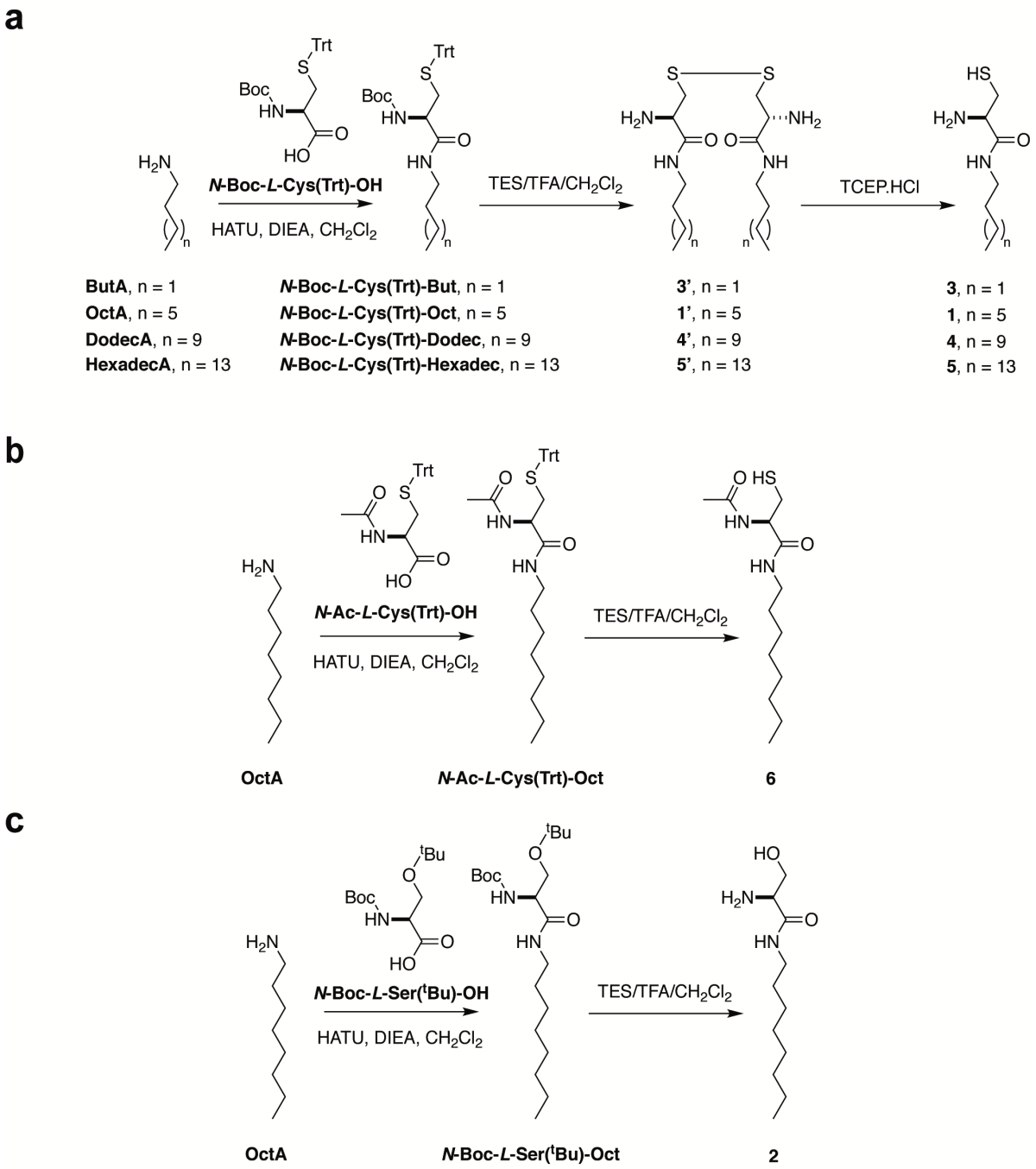

Scheme 2.1 Synthesis of Alkyl Cysteine Derivatives. **(a)** Synthesis of H_2N-*L*-Cys-But (**3**), H_2N-*L*-Cys-Oct (**1**), H_2N-*L*-Cys-Dodec (**4**) and H_2N-*L*-Cys-Hexadec (**5**). **(b)** Synthesis *N*-Ac-*L*-Cys-Oct (**6**). **(c)** Synthesis of H_2N-*L*-Ser-Oct (**2**). [ButA: butylamine, OctA: octylamine, DodecA: dodecylamine, HexadecA: hexadecylamine].

2.6.2 Synthesis of H_2N-*L*-Cys-Oct (1)

H_2N-*L*-Ser-Oct (2) was synthesized as before[21].

2.6.3 Synthesis of H_2N-*L*-Ser-Oct (2)

H_2N-*L*-Cys-Oct (1) was synthesized as before[21].

2.6.4 Synthesis of *N*-Boc-*L*-Cys(Trt)-But.

A solution of *N*-Boc-*L*-Cys(Trt)-OH (125.0 mg, 269.6 μmol) in CH_2Cl_2 (2.5 mL) was stirred at 0 ºC for 10 min, and then HATU (112.8 mg, 296.6 μmol) and DIEA (187.9 μL, 1.08 mmol) were successively added. After 10 min stirring at 0 ºC, butylamine (26.7 μL, 269.6 μmol) was added. After 1 h stirring at rt, the reaction mixture was washed with HCl(5%) (3 × 1 mL) and $NaHCO_3$(sat) (3 × 1 mL). The organic layer was dried (Na_2SO_4), filtered and concentrated, providing a yellow oil, which was purified by flash chromatography (0–4% MeOH in CH_2Cl_2), affording 136.8 mg of *N*-Boc-*L*-Cys(Trt)-But as a white solid [98%, R_f = 0.21 (1% MeOH in CH_2Cl_2)]. ^{1}H NMR ($CDCl_3$, 500.13 MHz, δ): 7.42 (dd, J_1 = 8.4 Hz, J_2 = 1.4 Hz, 6H, 6 × CH_{Ar}), 7.29 (dd, J_1 = 8.5 Hz, J_2 = 6.8 Hz, 6H, 6 × CH_{Ar}), 7.24–7.19 (m, 3H, 3 × CH_{Ar}), 5.98 (t, J = 6.0 Hz, 1H, 1 × NH), 4.96–4.70 (m, 1H, 1 × NH), 4.00–3.68 (m, 1H, 1 × CH), 3.28–3.08 (m, 2H, 1 × CH_2), 2.78–2.64 (m, 1H, 0.5 × CH_2), 2.56–2.42 (m, 1H, 0.5 × CH_2), 1.46–1.42 (m, 2H, 1 × CH_2), 1.41 (s, 9H, 3 × CH_3), 1.35–1.22 (m, 2H, 1 × CH_2), 0.88 (t, J = 7.3 Hz, 3H, 1 × CH_3). ^{13}C NMR ($CDCl_3$, 125.77 MHz, δ): 170.4, 155.5, 144.5, 129.7, 128.2, 127.0, 80.3, 67.3, 53.7, 39.3, 38.8, 31.5, 28.4, 20.1, 13.8. MS (ESI-TOF) [m/z (%)]: 541 ([M +Na]$^+$, 100).

2.6.5 Synthesis of H_2N-*L*-Cys-But ∪ H_2N-*L*-Cys-But (3').*

A solution of *N*-Boc-*L*-Cys(Trt)-But (50.0 mg, 96.5 μmol) in 500 μL of TFA/CH_2Cl_2/TES (225:225:50) was stirred at rt for 30 min. After removal of the solvent, the residue was dried under

high vacuum for 3 h. Then, the corresponding residue was diluted in MeOH (250 μL), filtered using a 0.2 μm syringe-driven filter, and the crude solution was purified by HPLC, affording 11.7 mg of the H_2N-*L*-Cys-But ∪ H_2N-*L*-Cys-But (**3'**) as a colorless film [69%, t_R = 7.5 min (Zorbax SB-C18 semipreparative column, 90–10% *Phase A* in *Phase B*, 15 min)]. As a disulfide (RS-SR): t_R = 0.86 min (Eclipse Plus C8 analytical column, 5% *Phase A* in *Phase B*, 5.5 min), or t_R = 4.52 min (Eclipse Plus C8 analytical column, 95–5% *Phase A* in *Phase B*, 5.5 min). ^{1}H NMR (CD_3OD, 500.13 MHz, δ): 4.12–3.94 (m, 2H, 2 × CH), 3.30–3.19 (m, 6H, 2 × CH_2 + 2 × CH), 3.11–2.95 (m, 2H, 2 × CH), 1.63–1.46 (m, 4H, 2 × CH_2), 1.45–1.33 (m, 4H, 2 × CH_2), 0.95 (t, *J* = 7.3 Hz, 6H, 2 × CH_3). ^{13}C NMR (CD_3OD, 125.77 MHz, δ): 169.9, 53.5, 40.6, 40.5, 32.4, 21.1, 14.1. MS (ESI-TOF) [m/z (%)]: 351 ([MH]$^+$, 100]. HRMS (ESI-TOF) calculated for [$C_{14}H_{30}N_4O_2S_2$] ([M +Na]$^+$) 373.1702, found 373.1698.

* Air oxidation of the thiol (RSH) causes the disulfide bond (RS-SR) formation

2.6.6 Synthesis of H_2N-*L*-Cys-But (3).

A solution of H_2N-*L*-Cys-But ∪ H_2N-*L*-Cys-But (**3'**, 1.0 mg, 2.9 μmol) in 1.14 mL of a 5 mM solution of TCEP.HCl in H_2O (or DMSO) was stirred at rt for 5 min. Then, it was analyzed by HPLC and/or used directly for the depalmitoylation experiments. As a free thiol (R-SH): t_R = 0.79 min (Eclipse Plus C8 analytical column, 5% *Phase A* in *Phase B*, 5.5 min), or t_R = 3.89 min (Eclipse Plus C8 analytical column, 95–5% *Phase A* in *Phase B*, 5.5 min). MS (ESI-TOF) [m/z (%)]: 177 ([MH]$^+$, 100).

2.6.7 Synthesis of *N*-Boc-*L*-Cys(Trt)-Dodec.

A solution of *N*-Boc-*L*-Cys(Trt)-OH (125.0 mg, 269.6 μmol) in CH_2Cl_2 (2.5 mL) was stirred at 0 ºC for 10 min, and then HATU (112.8 mg, 296.6 μmol) and DIEA (187.9 μL, 1.08 mmol) were successively added. After 10 min stirring at 0 ºC, dodecylamine (50.0 mg, 269.6 μmol) was added.

After 1 h stirring at rt, the reaction mixture was washed with HCl(5%) (3 × 1 mL) and $NaHCO_3$(sat) (3 × 1 mL). The organic layer was dried (Na_2SO_4), filtered and concentrated, providing a yellow oil, which was purified by flash chromatography (0–3% MeOH in CH_2Cl_2), affording 163.8 mg of *N*-Boc-*L*-Cys(Trt)-Dodec as a pale yellow oil [96%, R_f = 0.52 (1% MeOH in CH_2Cl_2)]. ^{1}H NMR ($CDCl_3$, 500.13 MHz, δ): 7.50–7.36 (m, 6H, 6 × CH_{Ar}), 7.28 (dd, J_1 = 8.5 Hz, J_2 = 6.9 Hz, 6H, 6 × CH_{Ar}), 7.24–7.19 (m, 3H, 3 × CH_{Ar}), 5.98 (d, J = 5.8 Hz, 1H, 1 × NH), 4.90–4.71 (m, 1H, 1 × NH), 3.90–3.74 (m, 1H, 1 × CH), 3.24–3.09 (m, 2H, 1 × CH_2), 2.77–2.65 (m, 1H, 0.5 × CH_2), 2.58–2.41 (m, 1H, 0.5 × CH_2), 1.47–1.42 (m, 2H, 1 × CH_2), 1.41 (s, 9H, 3 × CH_3), 1.34–1.14 (m, 18H, 9 × CH_2), 0.87 (t, J = 6.9 Hz, 3H, 1 × CH_3). ^{13}C NMR ($CDCl_3$, 125.77 MHz, δ): 170.3, 155.5, 144.5, 129.7, 128.2, 127.0, 80.3, 67.3, 53.7, 39.6, 38.7, 32.0, 29.8, 29.7, 29.7, 29.7, 29.5, 29.5, 29.4, 28.4, 27.0, 22.8, 14.3. MS (ESI-TOF) [m/z (%)]: 653 ([M +Na]$^+$, 100).

2.6.8 Synthesis of H_2N-*L*-Cys-Dodec ∪ H_2N-*L*-Cys-Dodec (4').*

A solution of *N*-Boc-*L*-Cys(Trt)-Dodec (50.0 mg, 79.3 μmol) in 500 μL of TFA/CH_2Cl_2/TES (225:225:50) was stirred at rt for 30 min. After removal of the solvent, the residue was dried under high vacuum for 3 h. Then, the corresponding residue was diluted in MeOH (250 μL), filtered using a 0.2 μm syringe-driven filter, and the crude solution was purified by HPLC, affording 16.8 mg of the H_2N-*L*-Cys-Dodec ∪ H_2N-*L*-Cys-Dodec (**4'**) as a colorless film [73%, t_R = 8.0 min (Zorbax SB-C18 semipreparative column, 50% *Phase A* in *Phase B*, 5 min, and then 5% *Phase A* in *Phase B*, 10 min)]. As a disulfide (RS-SR): t_R = 2.80 min (Eclipse Plus C8 analytical column, 5% *Phase A* in *Phase B*, 5.5 min). ^{1}H NMR (CD_3OD, 500.13 MHz, δ): 4.09–3.96 (m, 2H, 2 × CH), 3.30–3.19 (m, 6H, 2 × CH_2 + 2 × CH), 3.11–2.96 (m, 2H, 2 × CH), 1.63–1.49 (m, 4H, 2 × CH_2), 1.40–1.25 (m, 36H, 18 × CH_2), 0.90 (t, J = 6.9 Hz, 6H, 2 × CH_3). ^{13}C NMR (CD_3OD, 125.77 MHz, δ): 170.2, 53.6, 40.9, 40.9, 33.1, 30.9, 30.8, 30.8, 30.5, 30.5, 30.3, 28.1, 23.8, 14.5. MS (ESI-TOF)

[m/z (%)]: 575 ([MH]$^+$, 100]. HRMS (ESI-TOF) calculated for [$C_{30}H_{62}N_4O_2S_2Na$] ([M +Na]$^+$) 597.3206, found 597.4209.

* Air oxidation of the thiol (RSH) causes the disulfide bond (RS-SR) formation.

2.6.9 Synthesis of H_2N-*L*-Cys-Dodec (4).

A solution of H_2N-*L*-Cys-Dodec ∪ H_2N-*L*-Cys-Dodec (**4'**, 1.0 mg, 1.7 μmol) in 695.7 μL of a 5 mM solution of TCEP.HCl in H_2O (or DMSO) was stirred at rt for 5 min. Then, it was analyzed by HPLC and/or used directly for the depalmitoylation experiments. As a free thiol (R-SH): t_R = 2.67 min (Eclipse Plus C8 analytical column, 5% *Phase A* in *Phase B*, 5.5 min). MS (ESI-TOF) [m/z (%)]: 289 ([MH]$^+$, 100).

2.6.10 Synthesis of *N*-Boc-*L*-Cys(Trt)-Hexadec.

A solution of *N*-Boc-*L*-Cys(Trt)-OH (125.0 mg, 269.6 μmol) in CH_2Cl_2 (2.5 mL) was stirred at 0 ºC for 10 min, and then HATU (112.8 mg, 296.6 μmol) and DIEA (187.9 μL, 1.08 mmol) were successively added. After 10 min stirring at 0 ºC, hexadecylamine (65.1 mg, 269.6 μmol) was added. After 1 h stirring at rt, the reaction mixture was washed with HCl(5%) (3 × 1 mL) and $NaHCO_3$(sat) (3 × 1 mL). The organic layer was dried (Na_2SO_4), filtered and concentrated, providing a yellow oil, which was purified by flash chromatography (0–3% MeOH in CH_2Cl_2), affording 180.7 mg of *N*-Boc-*L*-Cys(Trt)-Hexadec as a pale yellow oil [98%, R_f= 0.63 (1% MeOH in CH_2Cl_2)]. ^{1}H NMR ($CDCl_3$, 500.13 MHz, δ): 7.45–7.39 (m, 6H, 6 × CH_{Ar}), 7.29 (dd, J_1 = 8.6 Hz, J_2 = 6.9 Hz, 6H, 6 × CH_{Ar}), 7.24–7.18 (m, 3H, 3 × CH_{Ar}), 5.97 (d, J = 5.8 Hz, 1H, 1 × NH), 4.93–4.72 (m, 1H, 1 × NH), 3.92–3.73 (m, 1H, 1 × CH), 3.24–3.07 (m, 2H, 1 × CH_2), 2.78–2.64 (m, 1H, 0.5 × CH_2), 2.57–2.44 (m, 1H, 0.5 × CH_2), 1.47–1.42 (m, 2H, 1 × CH_2), 1.41 (s, 9H, 3 × CH_3), 1.32–1.20 (m, 26H, 13 × CH_2), 0.88 (t, J = 6.9 Hz, 3H, 1 × CH_3). ^{13}C NMR ($CDCl_3$, 125.77 MHz, δ): 170.3, 155.5, 144.5, 129.7, 128.2, 127.0, 80.3, 67.3, 53.7, 39.6, 38.8, 32.1, 29.8, 29.8,

29.8, 29.8, 29.7, 29.7, 29.5, 29.5, 29.4, 28.4, 27.0, 22.8, 14.3. MS (ESI-TOF) [m/z (%)]: 709 ([M +Na]$^+$, 100).

2.6.11 Synthesis of H_2N-*L*-Cys-Hexadec ∪ H_2N-*L*-Cys-Hexadec (5').*

A solution of *N*-Boc-*L*-Cys(Trt)-Hexadec (50.0 mg, 72.8 μmol) in 500 μL of TFA/CH_2Cl_2/TES (225:225:50) was stirred at rt for 30 min. After removal of the solvent, the residue was dried under high vacuum for 3 h. Then, the corresponding residue was diluted in MeOH (250 μL), filtered using a 0.2 μm syringe-driven filter, and the crude solution was purified by HPLC, affording 16.3 mg of the H_2N-*L*-Cys-Hexadec ∪ H_2N-*L*-Cys-Hexadec (**5'**) as a colorless film [65%, t_R = 8.9 min (Zorbax SB-C18 semipreparative column, 50% *Phase A* in *Phase B*, 5 min, and then 5% *Phase A* in *Phase B*, 10 min)]. As a disulfide (RS-SR): t_R = 3.13 min (Eclipse Plus C8 analytical column, 5% *Phase A* in *Phase B*, 5.5 min). ^{1}H NMR (CD_3OD, 500.13 MHz, δ): 4.06–3.95 (m, 2H, 2 × CH), 3.30–3.20 (m, 6H, 2 × CH_2 + 2 × CH), 3.09–2.95 (m, 2H, 2 × CH), 1.63–1.49 (m, 4H, 2 × CH_2), 1.37–1.26 (m, 52H, 26 × CH_2), 0.90 (t, *J* = 6.8 Hz, 6H, 2 × CH_3). ^{13}C NMR (CD_3OD, 125.77 MHz, δ): 170.4, 53.7, 41.0, 40.9, 33.1, 30.9, 30.8, 30.8, 30.5, 30.5, 30.3, 28.1, 23.8, 14.5. MS (ESI-TOF) [m/z (%)]: 687 ([MH]$^+$, 100]. HRMS (ESI-TOF) calculated for [$C_{38}H_{78}N_4O_2S_2Na$] ([M +Na]$^+$) 709.5458, found 709.5462.

* Air oxidation of the thiol (RSH) causes the disulfide bond (RS-SR) formation.

2.6.12 Synthesis of H_2N-*L*-Cys-Hexadec (5).

A solution of H_2N-*L*-Cys-Hexadec ∪ H_2N-*L*-Cys-Hexadec (**5'**, 1.0 mg, 1.5 μmol) in 582.1 μL of a 5 mM solution of TCEP.HCl in H_2O (or DMSO) was stirred at rt for 5 min. Then, it was analyzed by HPLC and/or used directly for the depalmitoylation experiments. As a free thiol (R-SH): t_R = 2.89 min (Eclipse Plus C8 analytical column, 5% *Phase A* in *Phase B*, 5.5 min). MS (ESI-TOF) [m/z (%)]: 345 ([MH]$^+$, 100).

2.6.13 Synthesis of *N*-Ac-*L*-Cys(Trt)-Oct.

A solution of *N*-Ac-*L*-Cys(Trt)-OH (109.3 mg, 269.6 μmol) in CH_2Cl_2 (2.5 mL) was stirred at 0 ºC for 10 min, and then HATU (112.8 mg, 296.6 μmol) and DIEA (187.9 μL, 1.08 mmol) were successively added. After 10 min stirring at 0 ºC, octylamine (44.6 mg, 269.6 μmol) was added. After 1 h stirring at rt, the reaction mixture was washed with HCl(5%) (3 × 1 mL) and $NaHCO_3$(sat) (3 × 1 mL). The organic layer was dried (Na_2SO_4), filtered and concentrated, providing a yellow oil, which was purified by flash chromatography (0–4% MeOH in CH_2Cl_2), affording 129.9 mg of *N*-Ac-*L*-Cys(Trt)-Oct as a white solid [93%, R_f = 0.11 (1% MeOH in CH_2Cl_2)]. ^{1}H NMR ($CDCl_3$, 500.13 MHz, δ): 7.45–7.40 (m, 6H, 6 × CH_{Ar}), 7.28 (dd, J_1 = 8.5 Hz, J_2 = 6.8 Hz, 6H, 6 × CH_{Ar}), 7.24–7.19 (m, 3H, 3 × CH_{Ar}), 6.04 (d, J = 6.0 Hz, 1H, 1 × NH), 5.95 (d, J = 6.0 Hz, 1H, 1 × NH), 4.07 (dt, J_1 = 7.6 Hz, J_2 = 6.4 Hz, 1H, 1 × CH), 3.23–3.04 (m, 2H, 1 × CH_2), 2.71 (ddd, J_1 = 12.9 Hz, J_2 = 6.8 Hz, J_3 = 1.4 Hz, 1H, 0.5 × CH_2), 2.51 (dd, J_1 = 13.0 Hz, J_2 = 6.0 Hz, 1H, 0.5 × CH_2), 1.88 (s, 3H, 1 × CH_3), 1.42 (t, J = 7.1 Hz, 2H, 1 × CH_2), 1.35–1.13 (m, 10H, 5 × CH_2), 0.86 (t, J = 6.9 Hz, 3H, 1 × CH_3). ^{13}C NMR ($CDCl_3$, 125.77 MHz, δ): 170.2, 170.0, 144.5, 129.7, 128.2, 127.0, 67.3, 52.3, 39.7, 38.8, 31.9, 29.4, 29.3, 29.3, 27.0, 23.3, 22.7, 14.2. MS (ESI-TOF) [m/z (%)]: 539 ([M +Na]$^+$, 100).

2.6.14 Synthesis of *N*-Ac-*L*-Cys-Oct (6').*

A solution of *N*-Ac-*L*-Cys(Trt)-Oct (50.0 mg, 96.8 μmol) in 500 μL of TFA/CH_2Cl_2/TES (225:225:50) was stirred at rt for 30 min. After removal of the solvent, the residue was dried under high vacuum for 3 h. Then, the corresponding residue was diluted in MeOH (250 μL), filtered using a 0.2 μm syringe-driven filter, and the crude solution was purified by HPLC, affording 15.2 mg of the *N*-Ac-*L*-Cys-Oct (**6'**) as a white solid [57%, t_R = 8.4 min (Zorbax SB-C18 semipreparative column, 50% *Phase A* in *Phase B*, 5 min, and then 5% *Phase A* in *Phase B*, 10

min)]. ^{1}H NMR (CD_3OD, 500.13 MHz, δ): 4.41 (dd, J_1 = 7.0 Hz, J_2 = 6.0 Hz, 1H, 1 × CH), 3.26–3.11 (m, 2H, 1 × CH_2), 2.84 (dd, J_1 = 13.8 Hz, J_2 = 6.0 Hz, 1H, 1 × CH), 2.76 (dd, J_1 = 13.8 Hz, J_2 = 7.1 Hz, 1H, 1 × CH), 2.01 (s, 3H, 1 × CH_3), 1.58–1.44 (m, 2H, 1 × CH_2), 1.37–1.23 (m, 10H, 5 × CH_2), 0.90 (t, J = 6.9 Hz, 3H, 1 × CH_3). ^{13}C NMR (CD_3OD, 125.77 MHz, δ): 173.4, 172.2, 57.3, 40.5, 33.0, 30.4, 30.4, 30.4, 28.0, 26.9, 23.8, 22.5, 14.5. As a free thiol (R-SH): t_R = 2.94 min (Eclipse Plus C8 analytical column, 5% *Phase A* in *Phase B*, 5.5 min). MS (ESI-TOF) [m/z (%)]: 275 ([MH]$^+$, 100). HRMS (ESI-TOF) calculated for [$C_{13}H_{26}N_2O_2SNa$] ([M +Na]$^+$) 297.1607, found 297.1604.

* HPLC-ELSD, NMR and MS showed that the product obtained was the thiol *N*-Ac-*L*-Cys-Oct (**6**) and not the expected disulfide *N*-Ac-*L*-Cys-Oct ∪ N-Ac-*L*-Cys-Oct (**6'**).

2.6.15 Synthesis of *N*-Ac-*L*-Cys-Oct (6)

A solution of the possible formed *N*-Ac-*L*-Cys-Oct ∪ *N*-Ac-*L*-Cys-Oct (**6'**, 1.0 mg, 1.8 μmol) in 731.5 μL of a 5 mM solution of TCEP.HCl in H_2O (or DMSO) was stirred at rt for 5 min. Then, it was analyzed by HPLC and/or used directly for the depalmitoylation experiments. As a free thiol (R-SH): t_R = 2.94 min (Eclipse Plus C8 analytical column, 5% *Phase A* in *Phase B*, 5.5 min). MS (ESI-TOF) [m/z (%)]: 275 ([MH]$^+$, 100). HRMS (ESI-TOF) calculated for [$C_{13}H_{26}N_2O_2SNa$] ([M +Na]$^+$) 297.1607, found 297.1604.

* As we mentioned above, HPLC-ELSD, NMR and MS showed that the product obtained was *N*-Ac-*L*-Cys-Oct (**6**). However, air oxidation of the thiol (RSH) over time could cause the disulfide bond (RS-SR) formation. Therefore, the product was treated with TCEP.HCl to be completely sure that we have the desired depalmitoylating agent (**6**).

2.7 Acknowledgements

We would like to thank S. Gutkind (UCSD) for his advice and suggestions as well as providing the Sk-Mel-28 melanoma cell line. H.D.V. was supported by the Molecular Biophysics Training Grant, NIH Grant T32 GM008326. This study was supported by grants from the National Institute of Health (DP2DK111801-01S2 and T32CA009523-33). Tissue Technology Shared Resources P30CA23100.

Chapter 2, in full, is a reprint of the material as it appears in the publication Vora, H. D., Johnson, M., Brea, R. J., Rudd, A. K., and Devaraj N. K. (2020) Inhibition of NRAS Signaling in Melanoma through Direct Depalmitoylation Using Amphiphilic Nucleophiles. *ACS Chem. Biol. 15*, 2079-2086. The dissertation author is the primary investigator and author of this paper.

2.8 References

(1) Wei, Z., and Liu, H. T. (2002) MAPK signal pathways in the regulation of cell proliferation in mammalian cells. *Cell Res. 12*, 9–18.

(2) Crespo, P., and León, J. (2000) Ras proteins in the control of the cell cycle and cell differentiation. *Cell. Mol. Life Sci. 57*, 1613–1636.

(3) Nakada, M., Niska, J. A., Tran, N. L., McDonough, W. S., and Berens, M. E. (2005) EphB2/R-ras signaling regulates glioma cell adhesion, growth, and invasion. *Am. J. Pathol. 167*, 565–576.

(4) Spandidos, D. A., Sourvinos, G., Tsatsanis, C., and Zafiropoulos, A. (2002) Normal ras genes: their onco-suppressor and pro-apoptotic functions (review). *Int. J. Oncol. 21*, 237–241.

(5) Giehl, K., Skripczynski, B., Mansard, A., Menke, A., and Gierschik, P. (2000) Growth factor-dependent activation of the Ras-Raf-MEK-MAPK pathway in the human pancreatic carcinoma cell line PANC-1 carrying activated K-ras: Implications for cell proliferation and cell migration. *Oncogene 19*, 2930–2942.

(6) Simanshu, D. K., Nissley, D. V., and McCormick, F. (2017) RAS Proteins and Their Regulators in Human Disease. *Cell 170*, 17–33.

(7) Papke, B., and Der, C. J. (2017) Drugging RAS: Know the enemy. *Science (80-.). 355*, 1158–1163.

(8) Ostrem, J. M., Peters, U., Sos, M. L., Wells, J. A., and Shokat, K. M. (2013) K-Ras(G12C) inhibitors allosterically control GTP affinity and effector interactions. *Nature 503*, 548–551.

(9) Ostrem, J. M. L., and Shokat, K. M. (2016) Direct small-molecule inhibitors of KRAS: From structural insights to mechanism-based design. *Nat. Rev. Drug Discov. 15*, 771–785.

(10) Samatar, A. A., and Poulikakos, P. I. (2014) Targeting RAS-ERK signalling in cancer: Promises and challenges. *Nat. Rev. Drug Discov. 13*, 928–942.

(11) Webb, Y., Hermida-Matsumoto, L., and Resh, M. D. (2000) Inhibition of protein palmitoylation, raft localization, and T cell signaling by 2-bromopalmitate and polyunsaturated fatty acids. *J. Biol. Chem. 275*, 261–270.

(12) Rajalingam, K., Schreck, R., Rapp, U. R., and Albert, S. (2007) Ras oncogenes and their downstream targets. *Biochim. Biophys. Acta - Mol. Cell Res. 1773*, 1177–1195.

(13) Ahearn, I. M., Haigis, K., Bar-Sagi, D., and Philips, M. R. (2012) Regulating the regulator: Post-translational modification of RAS. *Nat. Rev. Mol. Cell Biol. 13*, 39–51.

(14) Xiang, S., Bai, W., Bepler, G., and Zhang, X. (2017) Activation of Ras by Post-Translational Modifications. *Conqu. RAS*. Elsevier Inc.

(15) Resh, M. D. (2012) Targeting protein lipidation in disease. *Trends Mol. Med. 18*, 206–214.

(16) Yeste-Velasco, M., Linder, M. E., and Lu, Y. J. (2015) Protein S-palmitoylation and cancer. *Biochim. Biophys. Acta - Rev. Cancer 1856*, 107–120.

(17) Gajewski, T. F., Salama, A. K. S., Niedzwiecki, D., Johnson, J., Linette, G., Bucher, C., Blaskovich, M. A., Sebti, S. M., and Haluska, F. (2012) Phase II study of the farnesyltransferase inhibitor R115777 in advanced melanoma (CALGB 500104). *J. Transl. Med. 10*, 1–8.

(18) Berndt, N., Hamilton, A. D., and Sebti, S. M. (2011) Targeting protein prenylation for cancer therapy. *Nat. Rev. Cancer 11*, 775–791.

(19) Mikic, I., Planey, S., Zhang, J., Ceballos, C., Seron, T., von Massenbach, B., Watson, R., Callaway, S., McDonough, P. M., Price, J. H., Hunter, E., and Zacharias, D. (2006) A Live Cell, Image-Based Approach to Understanding the Enzymology and Pharmacology of 2-Bromopalmitate and Palmitoylation. *Methods Enzymol. 414*, 150–187.

(20) Davda, D., Azzouny, M. A. El, Tom, C. T. M. B., Jeannie, L., Majmudar, J. D.,

Kennedy, R. T., and Martin, B. R. (2014) Profiling targets of the irreversible palmitoylation inhibitor 2- bromopalmitate. *ACS Chem. Biol. 8*, 1912–1917.

(21) Rudd, A. K., Brea, R. J., and Devaraj, N. K. (2018) Amphiphile-Mediated Depalmitoylation of Proteins in Living Cells. *J. Am. Chem. Soc. 140*, 17374–17378.

(22) Ahmed, R. L., Shaughnessy, D. P., Knutson, T. P., Vogel, R. I., Ahmed, K., Kren, B. T., and Trembley, J. H. (2019) CDK11 loss induces cell cycle dysfunction and death of BRAF and NRAS Melanoma Cells. *Pharmaceuticals 12*, 1–20.

(23) Reyes-Uribe, P., Adrianzen-Ruesta, M. P., Deng, Z., Echevarria-Vargas, I., Mender, I., Saheb, S., Liu, Q., Altieri, D. C., Murphy, M. E., Shay, J. W., Lieberman, P. M., and Villanueva, J. (2018) Exploiting TERT dependency as a therapeutic strategy for NRAS-mutant melanoma. *Oncogene 37*, 4058–4072.

(24) Forrester, M. T., Hess, D. T., Thompson, J. W., Hultman, R., Moseley, M. A., Stamler, J. S., and Casey, P. J. (2011) Site-specific analysis of protein *S* -acylation by resin-assisted capture. *J. Lipid Res. 52*, 393–398.

(25) Howie, J., Reilly, L., Fraser, N. J., Vlachaki Walker, J. M., Wypijewski, K. J., Ashford, M. L. J., Calaghan, S. C., McClafferty, H., Tian, L., Shipston, M. J., Boguslavskyi, A., Shattock, M. J., and Fuller, W. (2014) Substrate recognition by the cell surface palmitoyl transferase DHHC5. *Proc. Natl. Acad. Sci. 111*, 17534–17539.

(26) Cuiffo, B., and Ren, R. (2010) Palmitoylation of oncogenic NRAS is essential for leukemogenesis. *Blood 115*, 3598–3605.

(27) Xu, J., Hedberg, C., Dekker, F. J., Li, Q., Haigis, K. M., Hwang, E., Waldmann, H., and Shannon, K. (2012) Inhibiting the palmitoylation/depalmitoylation cycle selectively reduces the growth of hematopoietic cells expressing oncogenic Nras. *Blood 119*, 1032–1035.

(28) Rocks, O., Gerauer, M., Vartak, N., Koch, S., Huang, Z. P., Pechlivanis, M., Kuhlmann, J., Brunsveld, L., Chandra, A., Ellinger, B., Waldmann, H., and Bastiaens, P. I. H. (2010) The palmitoylation machinery is a spatially organizing system for peripheral membrane proteins. *Cell 141*, 458–471.

(29) Song, S. P., Hennig, A., Schubert, K., Markwart, R., Schmidt, P., Prior, I. A., Böhmer, F. D., and Rubio, I. (2013) Ras palmitoylation is necessary for N-Ras activation and signal propagation in growth factor signalling. *Biochem. J. 454*, 323–332.

(30) Mendoza, M. C., Er, E. E., and Blenis, J. (2011) The Ras-ERK and PI3K-mTOR pathways: Cross-talk and compensation. *Trends Biochem. Sci. 36*, 320–328.

(31) Davies, H., Bignell, G. R., Cox, C., Stephens, P., Edkins, S., Clegg, S., Teague, J., Woffendin, H., Garnett, M. J., Bottomley, W., Davis, N., Dicks, E., Ewing, R., Floyd,

Y., Gray, K., Hall, S., Hawes, R., Hughes, J., Kosmidou, V., Menzies, A., Mould, C., Parker, A., Stevens, C., Watt, S., Hooper, S., Jayatilake, H., Gusterson, B. A., Cooper, C., Shipley, J., Hargrave, D., Pritchard-Jones, K., Maitland, N., Chenevix-Trench, G., Riggins, G. J., Bigner, D. D., Palmieri, G., Cossu, A., Flanagan, A., Nicholson, A., Ho, J. W. C., Leung, S. Y., Yuen, S. T., Weber, B. L., Seigler, H. F., Darrow, T. L., Paterson, H., Wooster, R., Stratton, M. R., and Futreal, P. A. (2002) Mutations of the BRAF gene in human cancer. *Nature 417*, 949–954.

(32) Ellerhorst, J. A., Greene, V. R., Ekmekcioglu, S., Warneke, C. L., Johnson, M. M., Cooke, C. P., Wang, L. E., Prieto, V. G., Gershenwald, J. E., Wei, Q., and Grimm, E. A. (2011) Clinical correlates of NRAS and BRAF mutations in primary human melanoma. *Clin. Cancer Res. 17*, 229–235.

(33) Woodfield, S. E., Zhang, L., Scorsone, K. A., Liu, Y., and Zage, P. E. (2016) Binimetinib inhibits MEK and is effective against neuroblastoma tumor cells with low NF1 expression. *BMC Cancer 16*, 1–10.

(34) Crassini, K., Shen, Y., Stevenson, W. S., Christopherson, R., Ward, C., Mulligan, S. P., and Best, O. G. (2018) MEK1/2 inhibition by binimetinib is effective as a single agent and potentiates the actions of Venetoclax and ABT-737 under conditions that mimic the chronic lymphocytic leukaemia (CLL) tumour microenvironment. *Br. J. Haematol. 182*, 360–372.

(35) Duchrow, M., Schlüter, C., Wohlenberg, C., Flad, H. D., and Gerdes, J. (1996) Molecular characterization of the gene locus of the human cell proliferation-associated nuclear protein defined by monoclonal antibody Ki-67. *Cell Prolif. 29*, 1–12.

(36) Eckle, V. S., Buchmann, A., Bursch, W., Schulte-Hermann, R., and Schwarz, M. (2004) Immunohistochemical Detection of Activated Caspases in Apoptotic Hepatocytes in Rat Liver. *Toxicol. Pathol. 32*, 9–15.

(37) Hadjiloucas, I., Gilmore, A. P., Bundred, N. J., and Streuli, C. H. (2001) Assessment of apoptosis in human breast tissue using an antibody against the active form of caspase 3: Relation to tumour histopathological characteristics. *Br. J. Cancer 85*, 1522–1526.

(38) Vincenzi, B., Armento, G., Spalato Ceruso, M., Catania, G., Leakos, M., Santini, D., Minotti, G., and Tonini, G. (2016) Drug-induced hepatotoxicity in cancer patients - implication for treatment. *Expert Opin. Drug Saf. 15*, 1219–1238.

(39) Suckow, M. A., Danneman, P., and Brayton, C. (2001) The Laboratory Mouse. CRC Press.

(40) Draper, J. M., and Smith, C. D. (2009) Palmitoyl acyltransferase assays and inhibitors (Review). *Mol. Membr. Biol. 26*, 5–13.

(41) Martin, B. R., and Cravatt, B. F. (2009) Large-scale profiling of protein palmitoylation in mammalian cells. *Nat. Methods 6*, 135–138.

(42) Jeng, H. H., Taylor, L. J., and Bar-Sagi, D. (2012) Sos-mediated cross-activation of wild-type Ras by oncogenic Ras is essential for tumorigenesis. *Nat. Commun. 3*, 1168.

(43) Margarit, S. M., Sondermann, H., Hall, B. E., Nagar, B., Hoelz, A., Pirruccello, M., Bar-Sagi, D., and Kuriyan, J. (2003) Structural evidence for feedback activation by Ras·GTP of the Ras-specific nucleotide exchange factor SOS. *Cell 112*, 685–695.

(44) Mátés, L., Chuah, M. K. L., Belay, E., Jerchow, B., Manoj, N., Acosta-Sanchez, A., Grzela, D. P., Schmitt, A., Becker, K., Matrai, J., Ma, L., Samara-Kuko, E., Gysemans, C., Pryputniewicz, D., Miskey, C., Fletcher, B., VandenDriessche, T., Ivics, Z., and Izsvák, Z. (2009) Molecular evolution of a novel hyperactive Sleeping Beauty transposase enables robust stable gene transfer in vertebrates. *Nat. Genet. 41*, 753–761.

(45) Kowarz, E., Löscher, D., and Marschalek, R. (2015) Optimized Sleeping Beauty transposons rapidly generate stable transgenic cell lines. *Biotechnol. J. 10*, 647–653.

(46) Woodfield, S. E., Zhang, L., Scorsone, K. A., Liu, Y., and Zage, P. E. (2016) Binimetinib inhibits MEK and is effective against neuroblastoma tumor cells with low NF1 expression. *BMC Cancer 16*, 1–10.

Chapter 3: Determination of SARS-CoV-2 Spike Glycoprotein Palmitoylation and its Contribution to Virus-Cell Fusion

3.1 Abstract

The emergence of the COVID-19 pandemic has made it more necessary than ever to better understand the molecular mechanism of viral entry and function that contributes to the spread and infectivity of the novel coronavirus SARS-CoV-2. Various viral proteins are post-translationally modified with palmitic acid, known as palmitoylation, including coronavirus spike glycoproteins. Palmitoylation has been determined to be essential for virus infectivity for a few coronaviruses, but the regions of palmitoylation and specific surface receptor interactions differs for each virus. It is currently unclear how palmitoylation of the novel SARS-CoV-2 spike protein contributes to virus-cell membrane fusion. This work focused on initially determining the essential sites of palmitoylation within the SARS-CoV-2 spike glycoprotein cysteine-rich C-terminal domain. I found that mutating the cysteine residues within Cluster 1 and Cluster 2 led to a decrease in palmitoylation levels compared to wildtype spike protein. Additionally, I studied the effects of palmitoylation inhibition, through pharmacological treatment or genetic mutation screening, on spike protein localization and membrane fusion. Although localization of the spike protein did not change with pharmacological or genetic manipulation, fewer membrane fusion events seemed to occur between the spike Cluster 1 mutant and the ACE2 receptor. This study sheds light on the role of palmitoylation on viral function and membrane fusion processes. In addition, this work can potentially lay the groundwork for the development of therapeutics that can target palmitoylation of SARS-CoV-2 spike protein as an approach to prevent virus-cell fusion and infectivity in humans.

3.2 Introduction

The COVID-19 pandemic that emerged at the end of 2019 has resulted in over 170 million confirmed cases and 3 million deaths worldwide[1]. COVID-19 is a respiratory disease that causes symptoms such as fever, dry cough, and shortness of breath[2]. This disease is caused by the novel coronavirus SARS-CoV-2, which is a positive-sense, single-stranded RNA virus[3]. All coronaviruses are known to encode three structural envelope proteins – spike glycoprotein (S), envelope protein (E), and membrane protein (M)[4,5]. The spike protein is the main protein in the viral membrane that facilitates virus-cell fusion by interacting with the ACE2 receptor on the surface of host cells[4]. The C-terminal cytoplasmic tail of the spike protein in coronaviruses, such as severe acute respiratory syndrome coronavirus (SARS-CoV) and mouse hepatitis virus (MHV), contain cysteine-rich regions that are S-palmitoylated by host cells[4,6,7].

S-palmitoylation is a cellular process where the 16-carbon saturated fatty acid palmitic acid is post-translationally attached to many endogenous cellular and viral proteins[8]. In particular, S-palmitoylation of viral proteins has been shown to have an important role in virus-host interactions[6,9]. Additionally, palmitoylation has a functional role in the entry of many viruses into host cells by spike-mediated membrane fusion[6]. Previous studies have determined that coronavirus spike protein palmitoylation is essential for spike-mediated virus-cell fusion, infectivity, and virus assembly[4,5]. However, past work has not characterized the functional role of spike protein palmitoylation on protein-protein interactions at the host cell surface. To this end, it is essential to study the basic function of spike protein palmitoylation in mediating viral processes.

Although palmitoylation of the spike protein is known to be required for viral assembly and infectivity in certain coronaviruses[6,7], it remains unclear what the molecular role of

palmitoylation is for the novel SARS-CoV-2 spike protein function. Additionally, the highly conserved nature of the spike protein cysteine-rich domain in coronaviruses and its clear role in membrane fusion and viral infectivity make it an attractive target for broad-spectrum antiviral development[4]. In order to develop therapeutic strategies to target the cysteine-rich palmitoylated regions of the novel SARS-CoV-2 spike glycoprotein, it is necessary to determine how depalmitoylation, through pharmacological or genetic means, affects spike-mediated cell fusion and spike protein interactions with host cell surface receptors.

Here, I aimed to determine the cysteine residues that are palmitoylated in the SARS-CoV-2 spike glycoprotein using site-directed mutagenesis and an acyl-resin-assisted capture (acyl-RAC) assay[10,11]. Next, I determined the effect on localization of these palmitoylation mutants and pharmacologically depalmitoylated spike protein compared to the wildtype spike protein using immunofluorescence. Additionally, I observed the change in spike-mediated virus-cell fusion using immunofluorescence to visualize formation of syncytia[4]. The information gained from this study can provide a basis to better understand the role of palmitoylation in viral protein function and potentially pave the way for developing better therapeutics that target palmitoylation of the spike glycoprotein in the novel coronavirus SARS-CoV-2.

3.3 Results

3.3.1 Palmitoylation of SARS-CoV-2 Spike Glycoprotein

I sought to determine the essential sites of palmitoylation on the SARS-CoV-2 spike glycoprotein as a starting point to understand its functional role on this important viral protein. To do so, full-length palmitoylation mutants of the spike glycoprotein were created using cloning methods. Various cluster mutants as well as site-specific mutants were made by mutating the

cysteine residues of interest to serine (Table 3.1). An acyl-resin assisted capture (acyl-RAC) assay was used to determine which cysteine residues are S-palmitoylated on the spike protein.

Initially, I wanted to observe the effects of pharmacological palmitoylation inhibition on total S-palmitoylation levels of the spike glycoprotein. To study the effects of inhibition on the full-length SARS-CoV-2 spike glycoprotein, cells were transiently transfected with wildtype spike protein and treated with increasing concentrations of 2-bromopalmitate (2-BP). 2-BP is an irreversible, non-specific palmitoylation inhibitor that is commonly used to study protein palmitoylation[12–14]. I did not observe a significant change in S-palmitoylation levels of the spike protein in a short treatment period of 2 h (Figure 3.1a,b). This result could have been due to the possibility that in a short period of time, there is no advantage for the spike protein to be depalmitoylated since viral proteins do not undergo endogenous enzymatic depalmitoylation[6]. However, after a longer 24 h treatment incubation, there was a dose-dependent decrease in spike protein palmitoylation (Figure 3.1c,d). These results suggest that inhibition of cellular palmitoyl acyltransferases (PATs) by 2-BP does influence spike protein palmitoylation in a dose-dependent and time-dependent manner.

To determine the specific cysteine residues that are essential for S-palmitoylation of the full-length spike glycoprotein, cells were transiently transfected with the various cluster mutants as well as the site-specific mutants (Table 3.1). The cysteine residues of interest within the C-terminal region were mutated to serine residues because of the structural similarities between the two amino acids and the fact that the alcohol group in the serine would be unable to be S-palmitoylated due to its chemical properties[15,16]. Using the acyl-RAC assay, I observed that the Cluster 1 and Cluster 2 palmitoylation mutants had an overall decrease in S-palmitoylation levels compared to that of the wildtype spike protein (Figure 3.2a,b). This suggests that the cysteine

residues in those two cluster regions may be S-palmitoylated. Additionally, a few of the site-specific palmitoylation mutants seemed to have a decrease in palmitoylation levels compared to the wildtype spike protein, such as the C1235S, C1241S, C1243S, and C1247S mutants (Figure 3.2a,c). It is interesting to note that these cysteine residues are within or near the Cluster 1 and Cluster 2 C-terminal regions.

Table 3.1. Palmitoylation Mutants in SARS-CoV-2 Spike Glycoprotein.

WT Spike C-terminal region = …CCMTSCCSCLKGCCSCGSCC…	
	Serine Mutants
Site 1 Mutant	…**S**CMTSCCSCLKGCCSCGSCC…
Site 2 Mutant	…C**S**MTSCCSCLKGCCSCGSCC…
Site 3 Mutant	…CCMTS**S**CSCLKGCCSCGSCC…
Site 4 Mutant	…CCMTSC**S**SCLKGCCSCGSCC…
Site 5 Mutant	…CCMTSCCS**S**LKGCCSCGSCC…
Site 6 Mutant	…CCMTSCCSCLKG**S**CSCGSCC…
Site 7 Mutant	…CCMTSCCSCLKGC**S**SCGSCC…
Site 8 Mutant	…CCMTSCCSCLKGCCS**S**GSCC…
Site 9 Mutant	…CCMTSCCSCLKGCCSCGS**S**C…
Site 10 Mutant	…CCMTSCCSCLKGCCSCGSC**S**…
Cluster 1 Mutant	…**SS**MTSCCSCLKGCCSCGSCC…
Cluster 2 Mutant	…CCMTS**SSS**LKGCCSCGSCC…
Cluster 3 Mutant	…CCMTSCCSCLKG**SS**S**S**GSCC…
Cluster 4 Mutant	…CCMTSCCSCLKGCCSCGS**SS**…
Full Region Mutant	…**SS**MTS**SSS**LKG**SSS**GS**SS**…

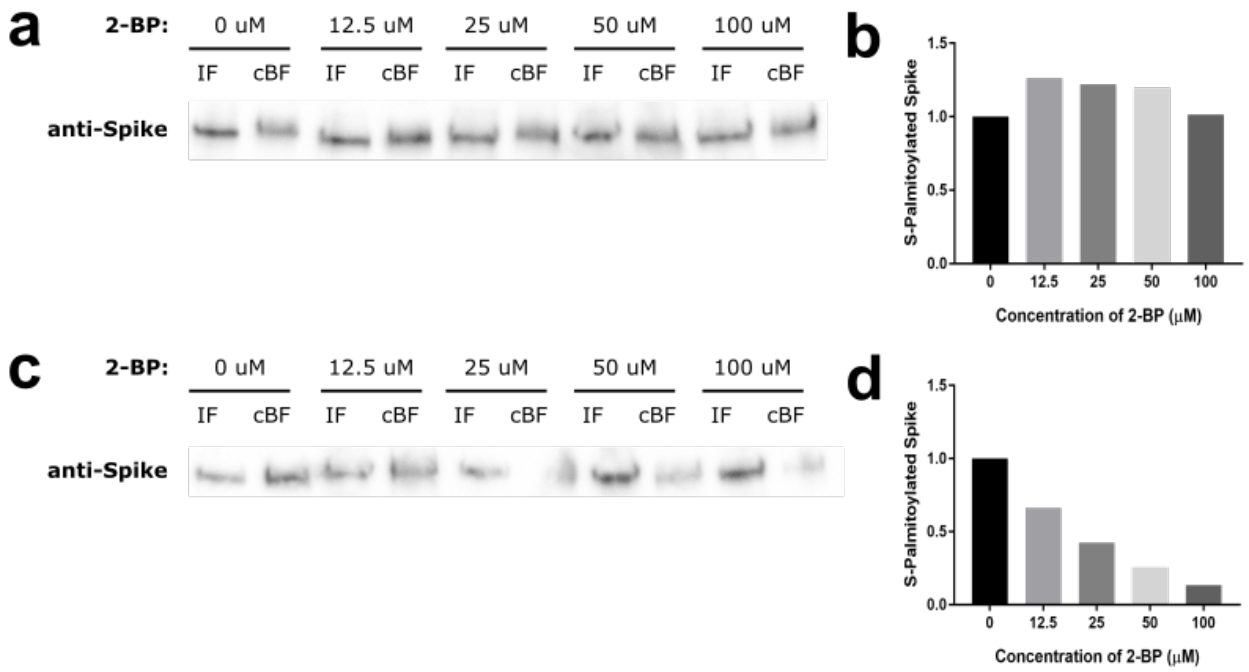

Figure 3.1 Palmitoylation Status of Spike Glycoprotein After Treatment with 2-BP. **(a)** Western blot detection of full-length spike protein in acyl-RAC fractions of HEK293T cells after 2 h treatment with increasing concentrations (0-100 μM) of 2-BP. Input fractions (IF) contain cellular protein and cleaved bound fractions (cBF) contain only S-palmitoylated proteins. **(b)** Western blot lanes were analyzed and quantified using ImageJ. Ratios of cBF to IF for each treatment condition was calculated and normalized to the 0 μM control to determine amount of S-palmitoylated spike protein in each sample. **(c)** Western blot detection of full-length spike protein after 24 h treatment with 2-BP. **(d)** Image analysis of western blot lanes.

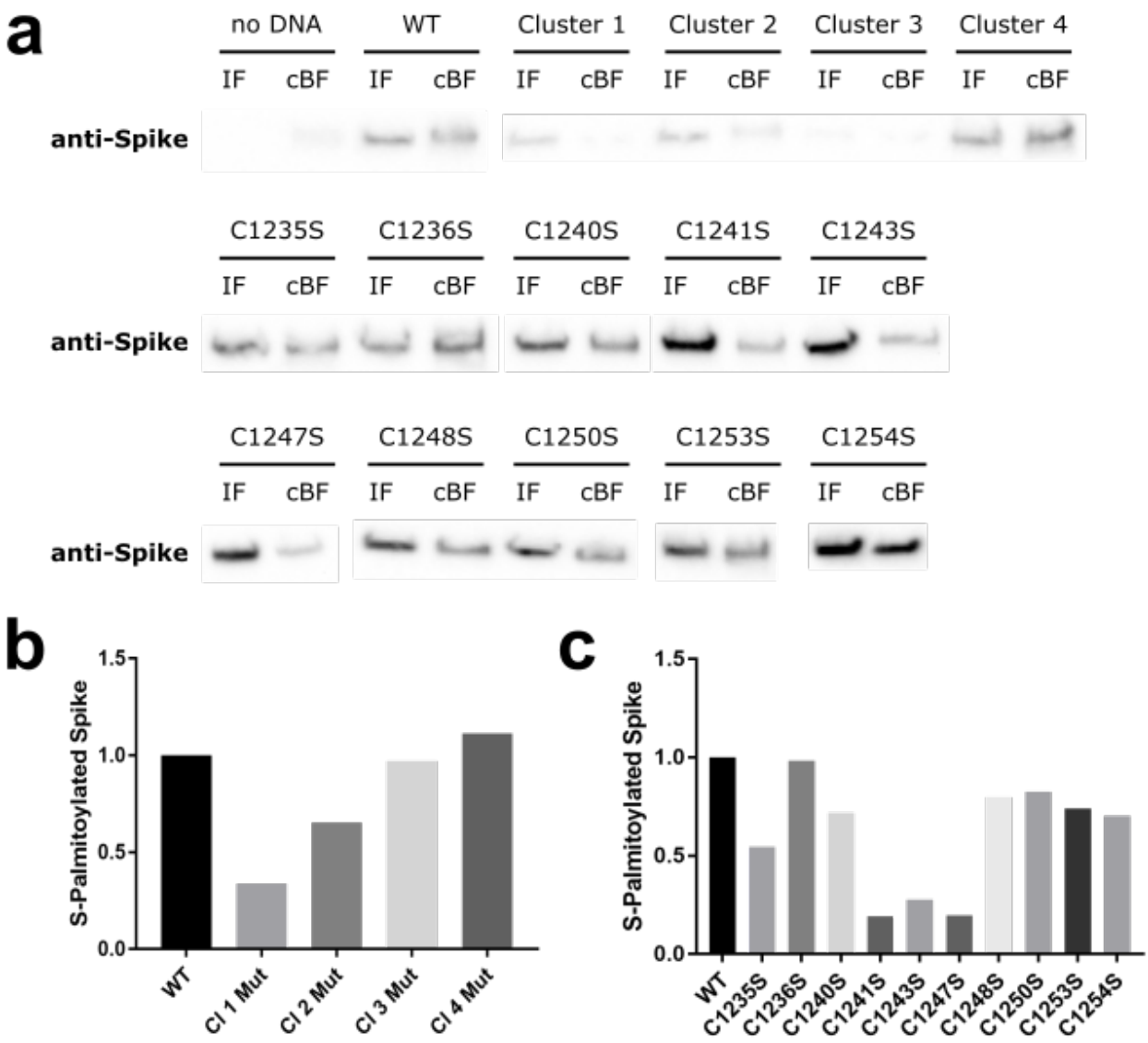

Figure 3.2 Palmitoylation Status of Spike Glycoprotein Palmitoylation Mutants. **(a)** Western blot detection of full-length spike protein in acyl-RAC fractions of HEK293T cells transiently transfected with various palmitoylation cluster and site-specific mutants. **(b)** Image analysis of western blot lanes of wildtype spike protein and cluster mutants. Ratios of cBF to IF for each mutant was calculated and normalized to the wildtype (WT) control to determine amount of S-palmitoylated spike protein in each sample. **(c)** Image analysis of western blot lanes of wildtype spike protein and site-specific mutants.

3.3.2 Localization and Membrane Fusion of SARS-CoV-2 Spike Glycoprotein

After determining that the SARS-CoV-2 spike glycoprotein is in fact S-palmitoylated at various sites within its cysteine-rich C-terminal domain, I aimed to study the effects of palmitoylation on spike localization as well as spike-mediated membrane fusion using immunofluorescence. Initially, I chose to observe the effects of the palmitoylation inhibitor 2-BP on the localization of the wildtype spike protein. Using an antibody for the SARS-CoV-2 spike glycoprotein, I observed that localization was unaffected even with increasing concentrations of 2-BP after a 24 h treatment period (Figure 3.3). This result suggested that spike protein membrane localization is not palmitoylation-dependent[4].

Next, I wanted to compare the results of pharmacological palmitoylation inhibition to genetic palmitoylation manipulation. Specifically, since palmitoylation inhibition after treatment with 2-BP did not have an observable effect on spike protein localization, I expected a similar result for the various SARS-CoV-2 spike glycoprotein palmitoylation cluster mutants. I did, in fact, observe that the localization of all the palmitoylation cluster mutants was similar to that of the wildtype spike protein (Figure 3.4a).

Although spike protein localization was unaltered regardless of pharmacological inhibition of palmitoylation or genetic mutation of palmitoylation sites, I aimed to determine if the membrane fusion events initiated by the spike glycoprotein were affected by these palmitoylation changes. Specifically, I conducted coculture experiments to observe the change in membrane fusion between cells transiently transfected with the spike protein palmitoylation cluster mutants and cells transiently transfected with the ACE2 receptor. Since the ACE2 receptor is the known binding partner of the SARS-CoV-2 spike protein that initiates viral fusion and entry, this coculture experiment was a valuable way to determine if membrane fusion is palmitoylation-dependent[4,16,17].

In particular, I used immunofluorescence to look for differences in syncytia formation or in the encapsulation of the spike expressing cells within the ACE2 receptor expressing cells. I observed a few differences in the membrane fusion of the cocultured cells compared to the fusion events that occurred between the wildtype spike transfected cells and the ACE2 receptor transfected cells. Cells expressing the Cluster 1 mutant seemed to have less membrane fusion and encapsulation events occurring between the cocultured cells compared to the fusion observed in the wildtype spike protein and other cluster mutants (Figure 3.4b). These results suggest that palmitoylation of the Cluster 1 region is necessary for the membrane fusion events that occur between the spike glycoprotein and the host ACE2 receptor.

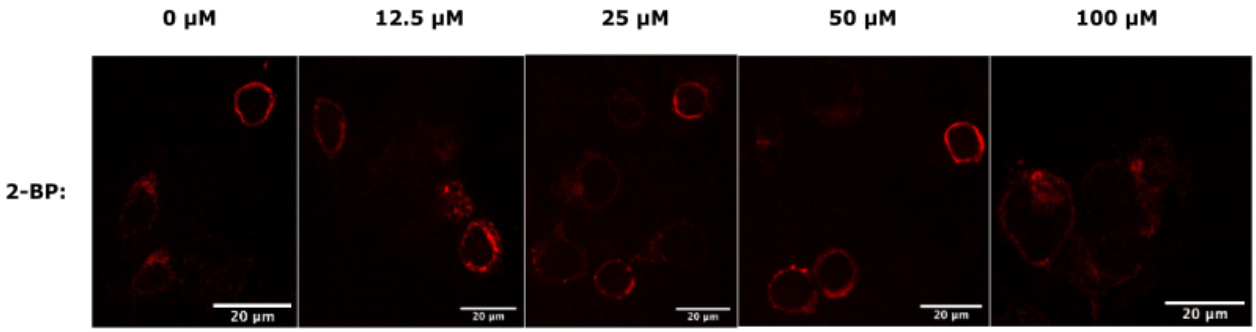

Figure 3.3 Localization of Spike Glycoprotein After Treatment with 2-BP. Immunofluorescence images of HEK293T cells transiently transfected with WT spike glycoprotein and treated with increasing concentrations (0-100 μM) of 2-BP for 24 h.

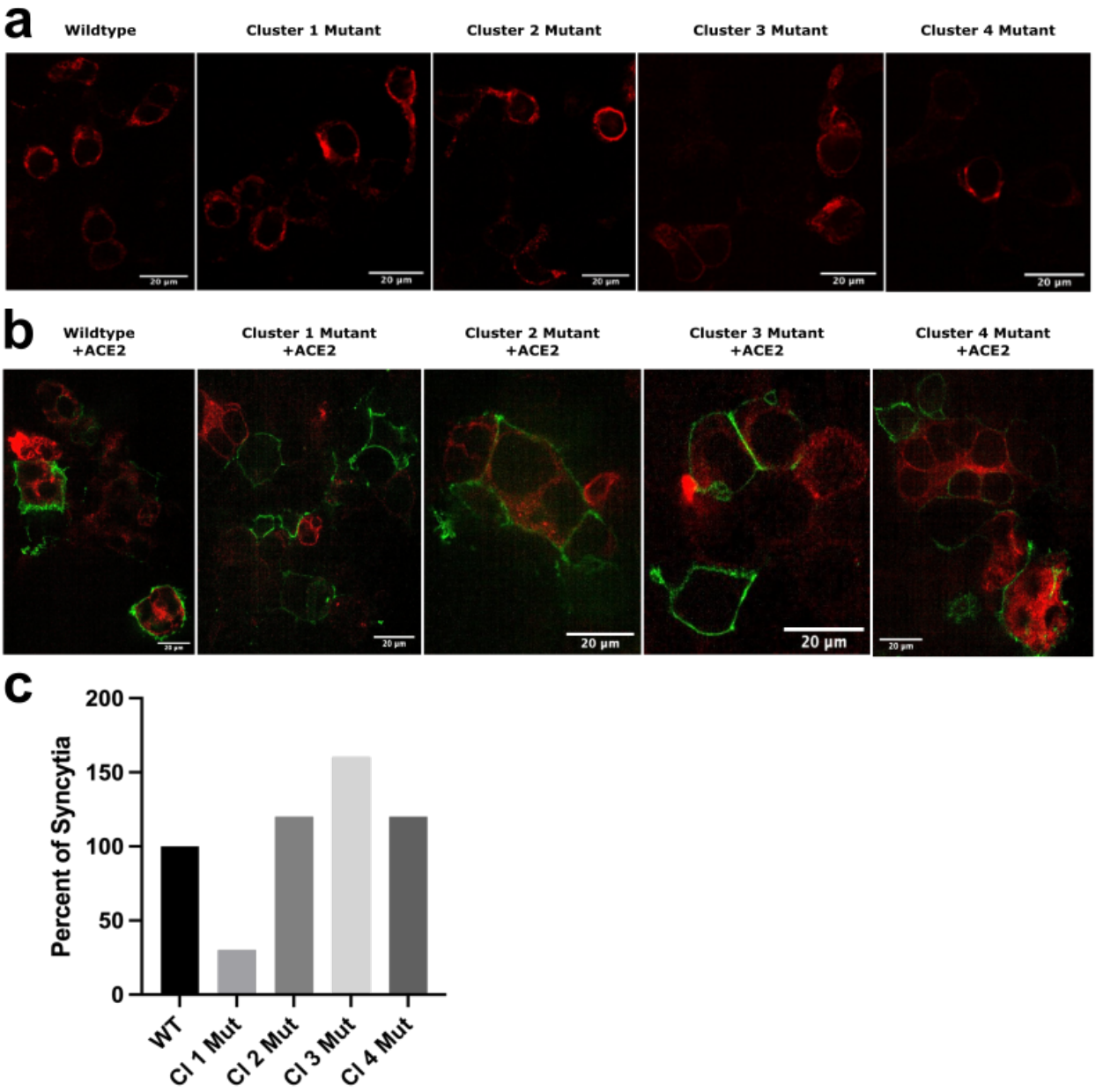

Figure 3.4 Localization and Membrane Fusion of Spike Glycoprotein Cluster Mutants. **(a)** Immunofluorescence images of HEK293T cells transiently transfected with spike glycoprotein cluster mutants. **(b)** Immunofluorescence images of HEK293T cells transiently transfected with spike glycoprotein cluster mutants (red; Alexa Fluor 594) cocultured with HEK293T cells transiently transfected with ACE2 receptor (green; Alexa Fluor 488). **(c)** Quantification of cell fusion from cocultured HEK293T cells in panel **b**. Image J was used to analyze syncytia formation within an area of 350 µm x 500 µm. Percentage of syncytia formation for each cluster mutant was calculated and normalized to wildtype (WT).

3.4 Discussion

The high incidence and mortality of COVID-19 worldwide has made it evident that there is great need for better therapeutics to combat this fatal disease. One potential approach would be to target the viral spike glycoprotein that initiates infection of the novel SARS-CoV-2 coronavirus. Previous studies have determined that the spike glycoprotein of various coronaviruses is palmitoylated[4,6]. However, there is still not much known about the effects of removing the palmitoylation modification from the spike protein as a potential antiviral therapeutic strategy. It would be valuable to explore the function of SARS-CoV-2 spike protein palmitoylation on viral processes that originate at the cell surface, such as membrane fusion, that could potentially be targeted.

In this study, I have determined the essential C-terminal cysteine residues and cluster regions on the SARS-CoV-2 spike glycoprotein that are S-palmitoylated. I also determined that inhibition of palmitoylation by 2-BP caused a decrease in spike protein S-palmitoylation levels in a dose-dependent manner after 24 h treatment. In addition, I observed that palmitoylation is not necessary for spike protein localization to the plasma membrane, while membrane fusion of the spike protein with the ACE2 receptor is palmitoylation-dependent. These results suggest that palmitoylation of the SARS-CoV-2 spike glycoprotein has an important role in virus-cell membrane fusion. Further studies are needed to better understand the contribution of spike protein palmitoylation to viral infectivity. Additionally, future directions include evaluating how protein-protein interactions between the spike glycoprotein and various host cell surface proteins are affected if the spike protein is depalmitoylated pharmacologically or unable to be palmitoylated by the palmitoylation mutants.

By understanding spike protein palmitoylation, alternative approaches to targeting the SARS-CoV-2 spike glycoprotein can be developed to overcome COVID-19. Considering the recent emergence of various strains and mutants of SARS-CoV-2, it would be beneficial to have various approaches to target the viral spike protein, which is known to initiate the fusion and entry of the virus into the host cell. The information gained from this study can contribute to antiviral drug discovery for the SARS-CoV-2 as well as other coronaviruses that may emerge in the future.

3.5 Acknowledgements

This study was supported by the National Science Foundation (NSF) Rapid Response Research (RAPID) grant (Award # 2031068).

3.6 References

(1) Dong, E., Du, H., and Gardner, L. (2020) An interactive web-based dashboard to track COVID-19 in real time. *Lancet Infect. Dis. 3099*, 19–20.

(2) Ibrahim, I. M., Abdelmalek, D. H., Elshahat, M. E., and Elfiky, A. A. (2020) COVID-19 spike-host cell receptor GRP78 binding site prediction. *J. Infect.*

(3) Gordon, D. E., Jang, G. M., Bouhaddou, M., Xu, J., Obernier, K., O'Meara, M. J., Guo, J. Z., Swaney, D. L., Tummino, T. A., Huttenhain, R., Kaake, R. M., Richards, A. L., Tutuncuoglu, B., Foussard, H., Batra, J., Haas, K., Modak, M., Kim, M., Haas, P., Polacco, B. J., Braberg, H., Fabius, J. M., Eckhardt, M., Soucheray, M., Bennett, M. J., Cakir, M., McGregor, M. J., Li, Q., Naing, Z. Z. C., Zhou, Y., Peng, S., Kirby, I. T., Melnyk, J. E., Chorba, J. S., Lou, K., Dai, S. A., Shen, W., Shi, Y., Zhang, Z., Barrio-Hernandez, I., Memon, D., Hernandez-Armenta, C., Mathy, C. J. P., Perica, T., Pilla, K. B., Ganesan, S. J., Saltzberg, D. J., Ramachandran, R., Liu, X., Rosenthal, S. B., Calviello, L., Venkataramanan, S., Liboy-Lugo, J., Lin, Y., Wankowicz, S. A., Bohn, M., Sharp, P. P., Trenker, R., Young, J. M., Cavero, D. A., Hiatt, J., Roth, T., Rathore, U., Subramanian, A., Noack, J., Hubert, M., Roesch, F., Vallet, T., Meyer, B., White, K. M., Miorin, L., Rosenberg, O. S., Verba, K. A., Agard, D., Ott, M., Emerman, M., Ruggero, D., Garc&iacute-Sastre, A., Jura, N., Zastrow, M. von, Taunton, J., Ashworth, A., Schwartz, O., Vignuzzi, M., D'Enfert, C., Mukherjee, S., Jacobson, M., Malik, H. S., Fujimori, D. G., Ideker, T., Craik, C. S., Floor, S., Fraser, J. S., Gross, J., Sali, A., Kortemme, T., Beltrao, P., Shokat, K., Shoichet, B. K., and

Krogan, N. J. (2020) A SARS-CoV-2-Human Protein-Protein Interaction Map Reveals Drug Targets and Potential Drug-Repurposing. *bioRxiv* 2020.03.22.002386.

(4) Petit, C. M., Chouljenko, V. N., Iyer, A., Colgrove, R., Farzan, M., Knipe, D. M., and Kousoulas, K. G. (2007) Palmitoylation of the cysteine-rich endodomain of the SARS-coronavirus spike glycoprotein is important for spike-mediated cell fusion. *Virology 360*, 264–274.

(5) McBride, C. E., and Machamer, C. E. (2010) Palmitoylation of SARS-CoV S protein is necessary for partitioning into detergent-resistant membranes and cell-cell fusion but not interaction with M protein. *Virology 405*, 139–148.

(6) Veit, M. (2012) Palmitoylation of virus proteins. *Biol. Cell 104*, 493–515.

(7) Fung, T. S., and Liu, D. X. (2018) Post-translational modifications of coronavirus proteins: Roles and function. *Future Virol. 13*, 405–430.

(8) Resh, M. D. (2006) Palmitoylation of ligands, receptors, and intracellular signaling molecules. *Sci. STKE 2006*, 1–15.

(9) Chen, B., Sun, Y., Niu, J., Jarugumilli, G. K., and Wu, X. (2018) Protein Lipidation in Cell Signaling and Diseases: Function, Regulation, and Therapeutic Opportunities. *Cell Chem. Biol. 25*, 817–831.

(10) Forrester, M. T., Hess, D. T., Thompson, J. W., Hultman, R., Moseley, M. A., Stamler, J. S., and Casey, P. J. (2011) Site-specific analysis of protein S-acylation by resin-assisted capture. *J. Lipid Res. 52*, 393–398.

(11) Howie, J., Reilly, L., Fraser, N. J., Vlachaki Walker, J. M., Wypijewski, K. J., Ashford, M. L. J., Calaghan, S. C., McClafferty, H., Tian, L., Shipston, M. J., Boguslavskyi, A., Shattock, M. J., and Fuller, W. (2014) Substrate recognition by the cell surface palmitoyl transferase DHHC5. *Proc. Natl. Acad. Sci. 111*, 17534–17539.

(12) Webb, Y., Hermida-Matsumoto, L., and Resh, M. D. (2000) Inhibition of protein palmitoylation, raft localization, and T cell signaling by 2-bromopalmitate and polyunsaturated fatty acids. *J. Biol. Chem. 275*, 261–270.

(13) Mikic, I., Planey, S., Zhang, J., Ceballos, C., Seron, T., von Massenbach, B., Watson, R., Callaway, S., McDonough, P. M., Price, J. H., Hunter, E., and Zacharias, D. (2006) A Live Cell, Image-Based Approach to Understanding the Enzymology and Pharmacology of 2-Bromopalmitate and Palmitoylation. *Methods Enzymol. 414*, 150–187.

(14) Davda, D., Azzouny, M. A. El, Tom, C. T. M. B., Jeannie, L., Majmudar, J. D., Kennedy, R. T., and Martin, B. R. (2014) Profiling targets of the irreversible palmitoylation inhibitor 2- bromopalmitate. *ACS Chem. Biol. 8*, 1912–1917.

(15) Vora, H. D., Johnson, M., Brea, R. J., Rudd, A. K., and Devaraj, N. K. (2020) Inhibition of NRAS Signaling in Melanoma through Direct Depalmitoylation Using Amphiphilic Nucleophiles. *ACS Chem. Biol. 15*, 2079–2086.

(16) Lee, M., Sugiyama, M., Mekhail, K., Latreille, E., Khosraviani, N., Wei, K., Lee, W. L., Antonescu, C., and Fairn, G. D. (2020) Fatty Acid Synthase inhibition prevents palmitoylation of SARS-CoV2 Spike Protein and improves survival of mice infected with murine hepatitis virus. *bioRxiv* 2020.12.20.423603.

(17) Hoffmann, M., Kleine-Weber, H., Schroeder, S., Krüger, N., Herrler, T., Erichsen, S., Schiergens, T. S., Herrler, G., Wu, N. H., Nitsche, A., Müller, M. A., Drosten, C., and Pöhlmann, S. (2020) SARS-CoV-2 Cell Entry Depends on ACE2 and TMPRSS2 and Is Blocked by a Clinically Proven Protease Inhibitor. *Cell* 1–10.